

Chem. Commun.

Four-colour response to self-sorting of mixed monolayer-protected metal nanoparticles

Sabrina Knospe,^a Marcus Koch,^b Birgit Nothdurft^c and Stefan Kubik^{*,a}

^a *Rheinland-Pfälzische Technische Universität Kaiserslautern-Landau, Fachbereich Chemie - Organische Chemie, Erwin-Schrödinger-Straße 54, 67663 Kaiserslautern, Germany.*

^b *Institute for Physical Process Technology, Saarland University of Applied Sciences, Göbenstr. 40, 66117 Saarbrücken, Germany*

^c *INM - Leibniz Institute for New Materials, Campus D2 2, 66123 Saarbrücken, Germany.*

CONTENT

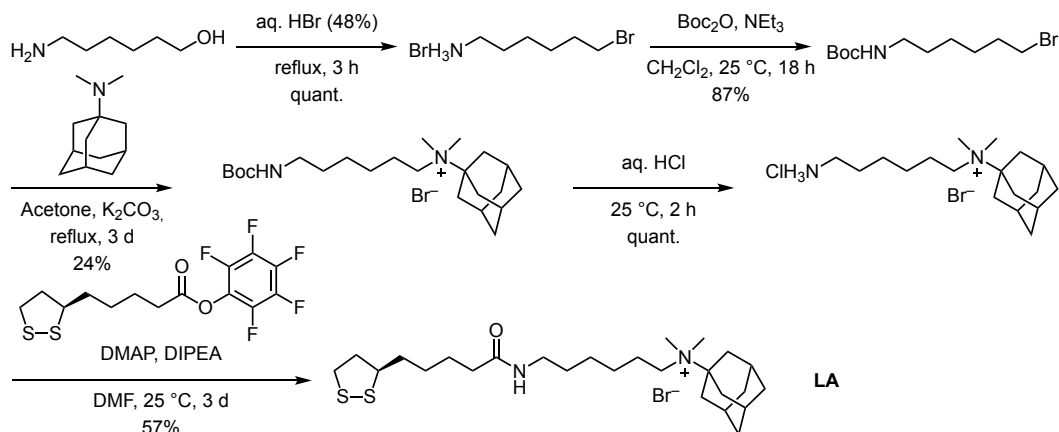
Syntheses of Compounds LA , LO , LG , baCD , and bβCD	S2
NMR and Mass Spectra of Compounds LA , LO , LG , baCD , and bβCD	S12
ITC and NMR titrations	S24
Nanoparticle Synthesis and Characterisation.....	S35
Binding Studies	S43
References.....	S62

Syntheses of Compounds LA, LO, LG, α CD, and β CD

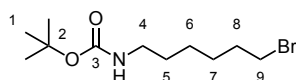
General details. Starting materials and reagents were commercially available and were used without further purification. Analyses were carried out as follows: ATR-IR, Perkin Elmer Spectrum 100 FT-IR-Spectrometer with Universal ATR Sampling Accessory Unit; ITC, Microcal VP-ITC; Centrifuge, Eppendorf Centrifuge 5702 R; Centrifugal Concentrators, Vivaspin® 15R (MWCO 5000 Da) Sartorius; elemental analysis, Elementar vario Micro cube; ESI-MS, Bruker Esquire 3000 Plus and Esquire 6000, Sciex Instruments TripleTOF 6600; APCI-MS, Advion Interchim Scientific Expression® CMS; NMR, Bruker AVANCE™ III 400 and 600 (peak assignments were confirmed by using H,H-COSY, HSQC and HMQC spectra, ^1H and ^{13}C NMR spectra were referenced to the residual solvent signals (CDCl_3 : $\delta^{\text{H}} = 7.26$ ppm, $\delta^{\text{C}} = 77.2$ ppm; $\text{DMSO}-d_6$: $\delta^{\text{H}} = 2.50$ ppm, $\delta^{\text{C}} = 39.52$ ppm, CD_3OD : $\delta^{\text{H}} = 3.31$ ppm, $\delta^{\text{C}} = 49.00$ ppm); melting points, Müller SPM-X 300; precision balance, Kern ABT 100-5M; preparative chromatography, silica gel 60 A (0.06-0.20 mm) Acros Organics; preparative HPLC, Dionex UltiMate 3000; column, Macherey Nagel Nucleodur HILIC, 250×21.2 mm, 5 μm particle size; temperature, 25 °C; flow, 10 mL/min; eluent, water/acetonitrile with the following gradient: 0-10 min, 100% acetonitrile; 10-15 min, 90% organic; 15-20 min, 80% organic; 20-30 min, linear decrease to 60% organic; 30-35 min, 40% organic; 35-46 min, 100% organic; reversed-phase chromatography, RP-8 POLYGOPREP® 60-50 C8 (40–63 μm) Macherey Nagel; TEM, JEOL JEM-2100 LaB6 Transmission Electron Microscope equipped with a Gatan Orius SC1000 CCD camera; UV-vis, Varian Cary 100.

The following abbreviations are used: AuNP, gold nanoparticle; AgNP, silver nanoparticles; DIPEA, ethyldiisopropylamine; DMAP, 4-dimethylaminopyridine; DMF, *N,N*-dimethylformamide; EDC, 1-ethyl-3-(3-dimethylaminopropyl)carbodiimide.

Synthesis of LA

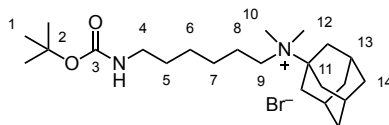


tert-Butyl-(6-bromohexyl)carbamate



6-Bromohexan-1-amine hydrobromide¹ (7.83 g, 30.0 mmol, 1 equiv) was suspended in dichloro methane (80 mL) and di-*tert*-butyl dicarbonate (6.88 g, 31.5 mmol, 1.05 equiv) and triethylamine (12.5 mL, 90 mmol, 3 equiv) were added under cooling. The solution was stirred for 18 h at 25 °C and then washed with water (3×50 mL). Imidazole (150 mg) was added to the organic phase, which was stirred for 30 min and washed again with water (3×50 mL). After drying with MgSO₄, the solvent was removed under reduced pressure. The product thus obtained was used without further purification. Yield: 7.31 g (26.1 mmol, 87%, brown oil); ¹H NMR (400 MHz, CDCl₃, 25 °C): δ = 4.49 (s, b, 1H, NH), 3.40 (t, ³J = 6.8 Hz, 2H, 9-H), 3.11 (t, ³J = 6.9 Hz, 2H, 4-H), 1.89-1.81 (m, 2H, 8-H), 1.60-1.25 (m, 15H, 1-H, 5-H, 6-H, 7-H) ppm; ¹³C NMR (101 MHz, CDCl₃, 25 °C): δ = 156.1 (3-C), 79.3 (2-C), 40.7 (4-C), 33.9 (9-C), 32.8 (8-C), 30.0 (5-C), 28.5 (1-C), 27.9 (7-C), 26.0 (6-C) ppm; MS (APCI+) *m/z* (%): 224.0 [M(⁷⁹Br)-C₄H₈+H]⁺ (100%), 226.0 [M(⁸¹Br)-C₄H₈+H]⁺ (98%), 180.0 [M(⁷⁹Br)-C₄H₈-CO₂+H]⁺ (1%), 182.0 [M(⁸¹Br)-C₄H₈-CO₂+H]⁺ (1%).

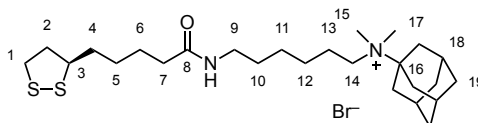
N-(*tert*-Butyloxycarbonylaminohexyl)-*N,N*-dimethyladamantylaminiumbromide



tert-Butyl-(6-bromohexyl)carbamate (3.85 g, 13.8 mmol, 1 equiv), *N,N*-dimethyladamantan-1-amine² (2.54 g, 14.2 mmol, 1.03 equiv), and anhydrous potassium carbonate (3.80 g, 27.5 mmol, 2

equiv) were suspended in acetone and the mixture was heated to reflux for 3 d. The solvent was removed and the residue suspended in MeCN. The solid was filtered off and the filtrate concentrated to 10 mL. The product was precipitated by the addition of diethyl ether. It was filtered off, washed with diethyl ether (2×50 mL) and dried in vacuo. Yield: 1.50 g (3.27 mmol, 24%, colourless solid); ¹H NMR (400 MHz, CD₃OD, 25 °C): δ = 3.26-3.22 (m, 2H, 9-H), 3.05 (t, ³J = 6.8 Hz, 2H, 4-H), 2.90 (s, 6H, 10-H), 2.33 (s, 3H, 13-H), 2.15-2.13 (m, 6H, 12-H), 1.85-1.70 (m, 8H, 8-H, 14-H), 1.51-1.43 (m, 15H, 1-H, 5-H, 6-H, 7-H) ppm; ¹³C NMR (101 MHz, CD₃OD, 25 °C): δ = 158.6 (3-C), 79.9 (2-C), 76.4 (11-C), 59.0 (9-C), 44.0 (10-C), 41.0 (4-C), 36.2 (14-C), 35.7 (12-C), 32.0 (13-C), 30.7 (1-C), 28.8 (7-C), 27.4, 27.3 (5-C, 6-C), 24.2 (8-C) ppm; MS (APCI⁺) *m/z* (%): 365.3 (100) [M–Br–CH₃+H]⁺; CHN calculated for C₂₃H₄₃BrN₂O₂ (M.W. 459.51) C, 60.12; H, 9.43; N, 6.10; found C, 59.78; H, 9.27; N, 6.09.

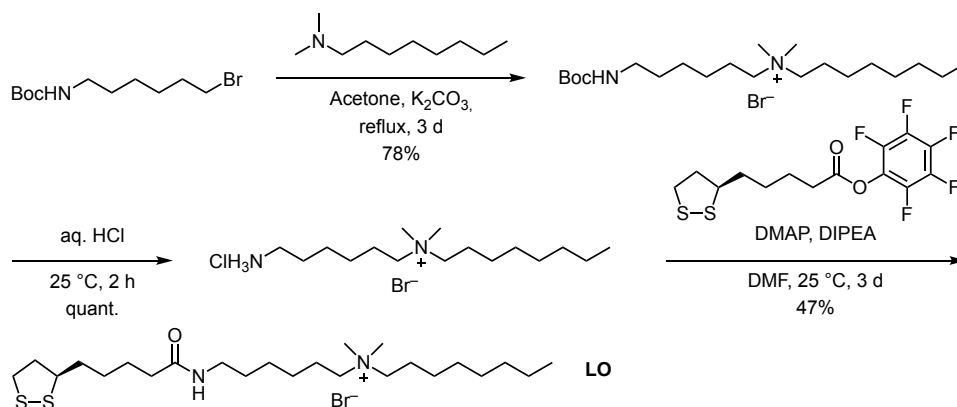
***N*-(6-(5-((*R*)-1,2-Dithiolan-3-yl)pentanamido)hexyl)-*N,N*-dimethyladamantylaminium bromide (LA)**



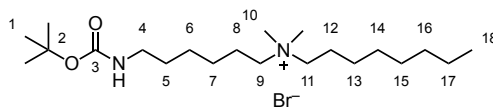
N-(*tert*-Butyloxycarbonylamino)hexyl)-*N,N*-dimethyladamantylaminiumbromide (2.30 g, 5.00 mmol, 1 equiv) was suspended in aqueous HCl (2 M, 10 mL) and the mixture was stirred for 2 h at room temperature. The solvent was removed under reduced pressure, the residue was suspended in DMF (20 mL) and DIPEA (3.50 mL, 20.0 mmol, 4 equiv) was added. Then, a solution of (*R*)-perfluorophenyl 5-(1,2-dithiolan-3-yl)pentanoate³ (2.05 g, 5.50 mmol, 1.1 equiv) and DMAP (122 mg, 1.0 mmol, 0.2 equiv) in DMF (20 mL) was added. The mixture was stirred at 25 °C for 3 d. Afterwards, the solvent was removed *in vacuo* and the residue was purified by column chromatography (RP-8, H₂O/MeCN, 9:1 → 6:1 → 4:1 (v/v)). Yield: 1.55 g (2.84 mmol, 57%, yellow resin); ¹H NMR (400 MHz, CD₃OD, 25 °C): δ = 3.60-3.56 (m, 1H, 3-H), 3.26-3.07 (m, 6H, 1-H, 9-H, 14-H), 2.90 (s, 6H, 15-H), 2.51-2.43 (m, 1H, 2-H), 2.37-2.29 (m, 3H, 18-H), 2.20 (t, ³J = 7.3 Hz, 2H, 7-H), 2.15-2.12 (m, 6H, 17-H), 1.93-1.85 (m, 1H, 2-H), 1.84-1.78 (m, 2H, 13-H), 1.78-1.74 (m, 6H, 19-H), 1.69-1.38 (m, 12H, 4-H, 5-H, 6-H, 10-H, 11-H, 12-H) ppm; ¹³C NMR (101 MHz, CD₃OD, 25 °C): δ = 176.0 (8-C), 76.4 (16-C), 59.0 (3-C), 57.7 (14-C), 44.1 (15-C), 41.4 (2-C), 40.0 (9-C),

39.4 (1-C), 36.9 (7-C), 36.2 (19-C), 35.7 (4-C, 17-C), 31.9 (18-C), 30.2 (10-C), 29.9 (5-C), 27.5 (12-C), 27.2 (11-C), 26.8 (13-C), 24.2 (6-C) ppm; MS (ESI+) m/z (%): 467.1 (100) $[M-Br]^+$; CHN calculated for $C_{26}H_{47}BrN_2OS_2 \cdot H_2O$ (M.W. 565.71) C, 55.20; H, 8.73; N, 4.95; S 11.33; found C, 55.0; H, 8.58; N, 4.97; S 11.09.

Synthesis of LO



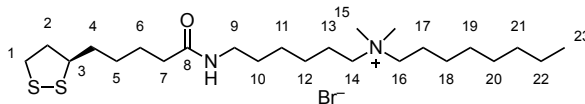
N-(*tert*-Butyloxycarbonylamino)hexyl)-*N,N*-dimethyloctan-1-aminiumbromide



tert-Butyl-(6-bromohexyl)carbamate (6.44 g, 23.0 mmol, 1 equiv) and commercially available *N,N*-dimethyloctan-1-amine (4.34 g, 27.6 mmol, 1.2 equiv) were dissolved in acetone and anhydrous K_2CO_3 (6.35 g, 46.0 mmol, 2 equiv) was added. The suspension was heated to reflux for 3 days and the solvent was removed under reduced pressure. The residue was suspended in acetonitrile, the solid was filtered off and the filtrate was evaporated to dryness. The resulting oil was dissolved in water (80 mL) and the aqueous layer was washed with diethyl ether (3×50 mL). The aqueous layer was evaporated to dryness under reduced pressure to yield pure product. Yield: 7.84 g (17.9 mmol, 78%, yellow resin); 1H NMR (400 MHz, CD_3OD , 25 °C): δ = 3.34-3.26 (m, 4H, 9-H, 11-H), 3.07 (s, 6H, 10-H), 3.04 (t, 3J = 7.0 Hz, 2H, 4-H), 1.82-1.70 (m, 4H, 8-H, 12-H), 1.54-1.46 (m, 2H, 5-H), 1.43 (s, 9H, 1-H), 1.42-1.29 (m, 14H, 6-H, 7-H, 13-H, 14-H, 15-H, 16-H, 17-H), 1.00-0.71 (m, 3H, 18-H) ppm; ^{13}C NMR (101 MHz, CD_3OD , 25 °C): δ = 158.5 (3-C), 79.7 (2-C), 65.4/65.2 (9-C, 11-C), 51.2 (10-C), 41.0 (4-C), 32.8 (16-C), 30.6/30.2/30.1 (5-C, 14-C, 15-C), 28.8 (1-C), 27.4/27.2/26.9 (6-C, 8-C, 12-C), 23.6/23.5/23.4 (7-C, 13-C, 17-C), 14.4 (18-C) ppm; MS (APCI+) m/z (%): 343.3 $[M-Br-$

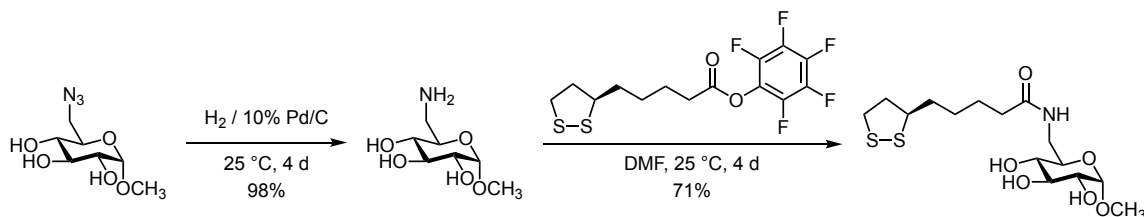
$\text{CH}_3 + \text{H}]^+$ (100%); CHN calculated for $\text{C}_{21}\text{H}_{45}\text{BrN}_2\text{O}_2 \cdot 0.5\text{H}_2\text{O}$ (M.W. 446.51) C, 56.49; H, 10.38; N, 6.27; found C, 56.28; H, 10.13; N, 6.32.

***N*-(6-(5-((*R*)-1,2-Dithiolan-3-yl)pentanamido)hexyl)-*N,N*-dimethyloctan-1-aminiumbromide (LO)**

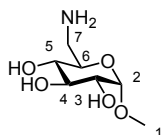


N-(*tert*-Butyloxycarbonylamino)hexyl)-*N,N*-dimethyloctan-1-aminiumbromide (3.22 g, 7.36 mmol) was suspended in aqueous HCl (2 M, 20 mL) and the mixture was stirred for 2 h at room temperature. The solvent was removed under reduced pressure, the residue was suspended in DMF (50 mL) and DIPEA (5.13 mL, 29.4 mmol, 4 equiv) was added. Then, a solution of (*R*)-perfluorophenyl 5-(1,2-dithiolan-3-yl)pentanoate³ (3.01 g, 8.10 mmol, 1.1 equiv) and DMAP (180 mg, 1.47 mmol, 0.2 equiv) in DMF (20 mL) was added. The mixture was stirred at 25 °C for 3 d. The solvent was removed *in vacuo* and the residue was purified by column chromatography [SiO_2 , $\text{CHCl}_3 \rightarrow \text{acetone} \rightarrow \text{CHCl}_3/\text{MeOH}$, 5:1 \rightarrow 3:1 (v/v)]. The residue remaining after evaporation of the fractions containing the product was dissolved in dichloromethane (50 mL) and the organic layer was washed with H_2O (3 \times 50 mL). After drying over MgSO_4 , the solvent was removed and the residue dried *in vacuo*. Yield: 1.82 g (3.46 mmol, 47%, yellow resin); ^1H NMR (400 MHz, CD_3OD , 25 °C): δ = 3.63-3.54 (m, 1H, 3-H), 3.30-3.24 (m, 4H, 1-H, 9-H), 3.24-3.12 (m, 4H, 14-H, 16-H), 3.10 (s, 6H, 15-H), 2.53-2.39 (m, 1H, 2-H), 2.23 (t, 3J = 7.3 Hz, 2H, 7-H), 1.97-1.89 (m, 1H, 2-H), 1.83-1.70 (m, 6H, 10-H, 13-H, 17-H), 1.69-1.49 (m, 4H, 4-H, 6-H), 1.49-1.27 (m, 16H, 5-H, 11-H, 12-H, 18-H, 19-H, 20-H, 21-H, 22-H), 0.98-0.80 (t, 3J = 6.7 Hz, 3H, 23-H) ppm; ^{13}C NMR (101 MHz, CD_3OD , 25 °C): δ = 175.9 (8-C), 65.4/65.3 (14-C, 16-C), 57.7 (3-C), 51.2 (15-C), 41.4 (2-C), 40.0/39.4 (1-C, 9-C), 36.9 (7-C), 35.7 (4-C), 32.9 (21-C), 30.3/30.2/30.1 (10-C, 19-C, 20-C), 29.9 (5-C), 27.4/27.3/27.0/26.8 (6-C, 11-C, 13-C, 17-C), 23.7/23.6/23.5 (12-C, 18-C, 22-C), 14.4 (23-C); MS (ESI+) m/z (%): 445.3 (100) [$\text{M}-\text{Br}]^+$; CHN calculated for $\text{C}_{24}\text{H}_{49}\text{BrN}_2\text{OS}_2 \cdot 0.25\text{H}_2\text{O}$ (M.W. 530.21) C, 54.37; H, 9.41; N, 5.28; S 12.10; found C, 54.50; H, 9.82; N, 5.58; S 11.71.

Synthesis of LG

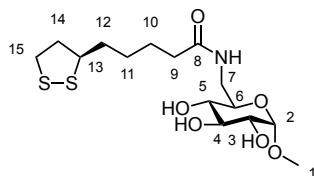


6-Amino-6-deoxy- α -methyl-D-glucopyranose



6-Azido-6-deoxy- α -methyl-D-glucopyranose⁴ (1.54 g, 7.00 mmol) was dissolved in methanol (40 mL). A suspension of 10% Pd/C (250 mg) in dichloromethane (5 mL) was added. The reaction mixture was stirred for 4 d under hydrogen at 25 °C. The catalyst was filtered off through celite and the filtrate was evaporated to dryness under reduced pressure. The residue was used without further purification. Yield: 1.33 g (6.86 mmol, 98%, colourless resin); ¹H NMR (400 MHz, CD₃OD, 25 °C): δ = 4.74 (d, ³J = 3.7 Hz, 1H, 2-H), 3.73 (td, ³J = 9.4, 3.0 Hz, 1H, 6-H), 3.61 (t, ³J = 9.2 Hz, 1H, 4-H), 3.45 (s, 3H, 1-H), 3.42 (dd, ³J = 9.7, 3.7 Hz, 3-H), 3.35 (dd, ²J = 13.1, ³J = 3.0 Hz, 1H, 7-H), 3.17 (t, ³J = 9.3 Hz, 1H, 5-H), 3.02 (dd, ²J = 13.0, ³J = 8.9 Hz, 1H, 7-H) ppm; ¹³C NMR (101 MHz, CH₃OD, 25 °C): δ = 101.4 (2-C), 74.5 (4-C), 73.3 (5-C), 73.1 (3-C), 69.2 (6-C), 56.3 (1-C), 42.2 (7-C) ppm; MS (APCI+) *m/z* (%): 144.0 (67) [M+H-CH₃OH-H₂O]⁺, 162.0 (100) [M+H-CH₃OH]⁺, 194.0 (63) [M+H]⁺, 370.2 (42) [M₂+H-NH₃]⁺.

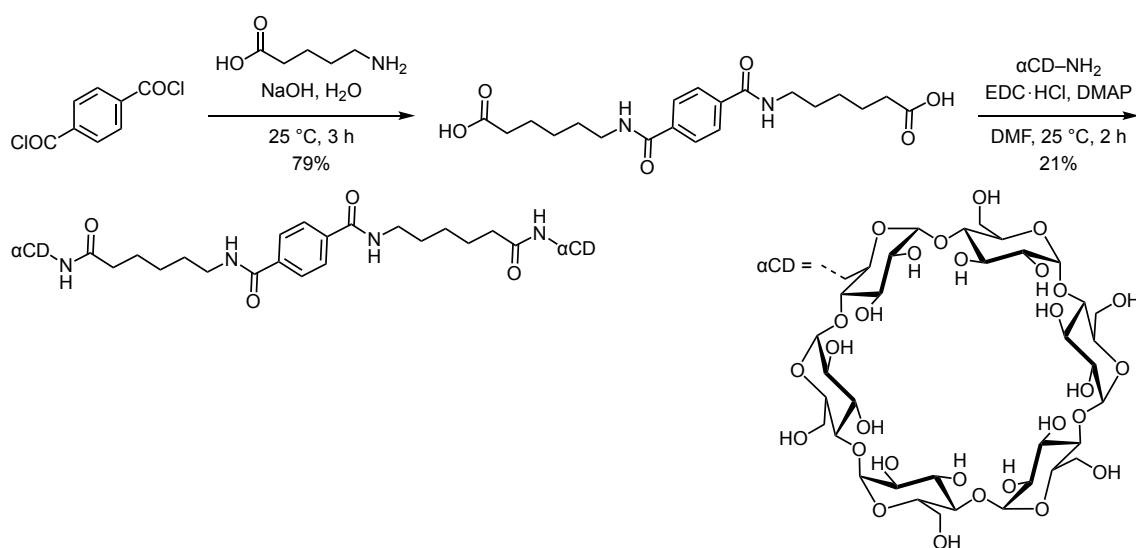
5-((*R*)-1,2-Dithiolan-3-yl)-N-(((2*R*,3*S*,4*S*,5*R*,6*S*)-3,4,5-trihydroxy-6-methoxytetrahydro-2H-pyran-2-yl)methyl)pentanamide (LG)



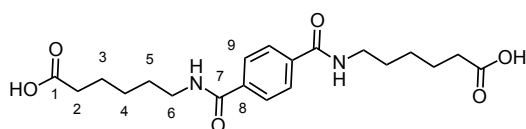
6-Amino-6-deoxy- α -methyl-D-glucopyranose (546 mg, 2.80 mmol, 1 equiv) and (*R*)-perfluorophenyl 5-(1,2-dithiolan-3-yl)pentanoate³ (1.12 g, 3.00 mmol, 1.1 equiv) were dissolved in DMF (25 mL), and the reaction mixture was stirred for 4 d at 25 °C. The solvent was removed under reduced pressure

and the residue was purified by column chromatography [RP-8, H₂O/MeCN, 9:1 → 4:1 → 1:1 (v/v)]. The product was dried *in vacuo*. Yield: 754 mg (1.98 mmol, 71%, yellow resin); ¹H NMR (400 MHz, CD₃OD, 25 °C): δ = 4.65 (d, ³J = 3.8 Hz, 1H, 2-H), 3.62-3.53 (m, 4H, 4-H, 6-H, 1×7-H, 13-H), 3.41-3.36 (m, 5H, 1-H, 3-H, 1×7-H), 3.21-3.07 (m, 3H, 5-H, 15-H), 2.50-2.42 (m, 1H, 14-H), 2.24 (t, ³J = 7.4 Hz, 2H, 9-H), 1.93-1.84 (m, 1H, 14-H), 1.77-1.60 (m, 4H, 10-H, 12-H), 1.54-1.42 (m, 2H, 11-H) ppm; ¹³C NMR (151 MHz, CD₃OD, 25 °C): δ = 176.6 (8-C), 101.3 (2-C), 74.6 (4-C), 73.6 (3-C), 73.2 (5-C), 71.7 (6-C), 57.6 (13-C), 55.6 (1-C), 41.4 (7-C), 41.3 (14-C), 39.3 (15-C), 36.8 (9-C), 35.8 (12-C), 29.9 (11-C), 26.8 (10-C) ppm; MS (ESI-MS) *m/z* (%): 332.2 (16%) [M-CH₃OH-H₂O+H]⁺, 350.2 (30%) [M-CH₃OH+H]⁺, 382.2 (100%) [M+H]⁺, 763.5 (21%) [M₂+H]⁺; CHN calculated for C₁₅H₂₇NO₆S₂·0.25H₂O (M.W. 386.01) C, 46.67; H, 7.18; N, 3.63; S 16.61; found C, 46.99; H, 7.39; N, 3.63; S 16.32.

Synthesis of βαCD



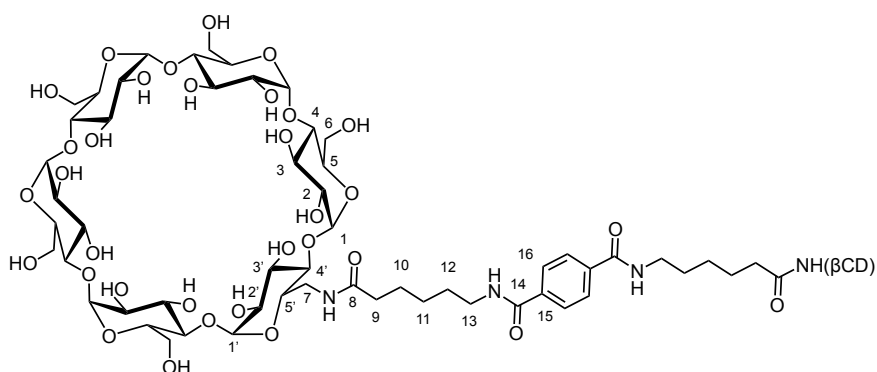
6,6'-(Terephthaloylbis(azanediyl))dihexanoic acid⁵



6-Aminohexanoic acid (2.62 g, 20.0 mmol, 2 eq.) was dissolved in aqueous NaOH (1M, 40 mL) and terephthalic acid dichloride (2.04 g, 10 mmol, 1 eq.) was added in portions. The suspension was stirred for 3 h at 25 °C. Water (60 mL) was added and the solid was filtered off. The filtrate was brought to pH 1 with aqueous sulfuric acid (20%), and the resulting solid was filtered off and washed with water.

The crude product was recrystallised from water/DMF (5:2 (v/v)). Yield: 3.08 g (7.85 mmol, 79%, colourless solid); mp: 259 °C; ^1H NMR (400 MHz, $\text{DMSO-}d_6$, 25 °C): δ = 8.57 (t, 3J = 5.7 Hz, 2H, NH), 7.89 (s, 4H, 9-H), 3.25 (t, 3J = 6.5 Hz, 4H, 6-H), 2.20 (t, 3J = 6.9 Hz, 4H, 2-H), 1.59-1.46 (m, 8H, 3-H, 5-H), 1.37-1.26 (m, 4H, 4-H) ppm; ^{13}C NMR (400 MHz, $\text{DMSO-}d_6$, 25 °C): δ = 174.5 (1-C), 165.4 (7-C), 136.7 (8-C), 127.1 (9-C), 39.0 (beneath $\text{DMSO-}d_6$ signal, from HSQC, 6-C), 33.7 (2-C), 28.8 (5-C), 26.1 (4-C), 24.3 (3-C) ppm; MS (APCI+) m/z (%): 393.3 $[\text{M}+\text{H}]^+$ (100%), 262.2 $[\text{M}-\text{C}_6\text{H}_{12}\text{NO}_2]^+$ (30%).

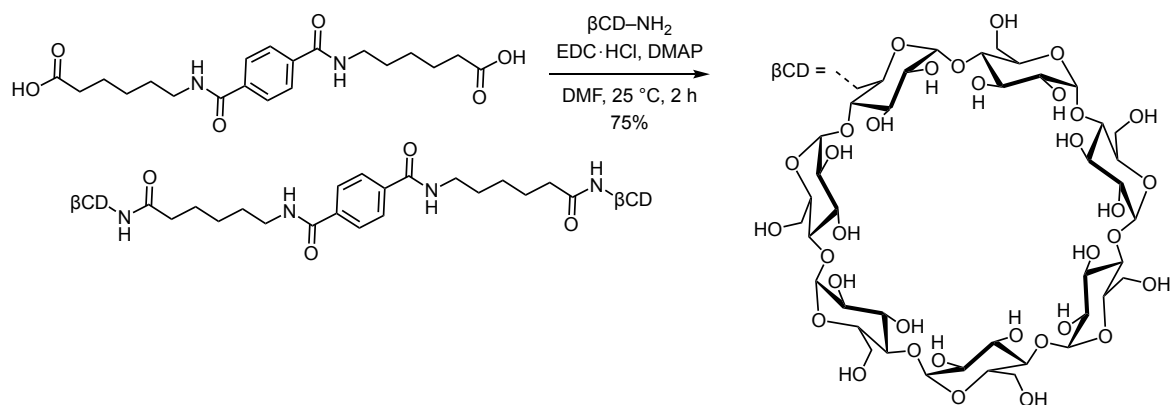
b α CD



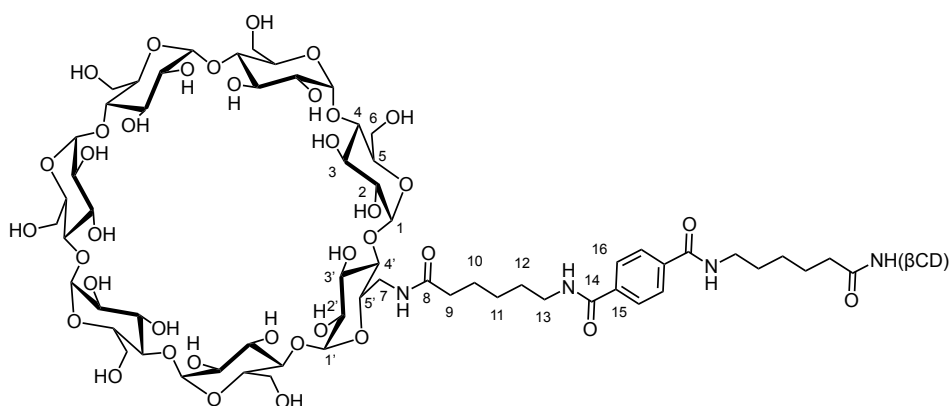
A solution of 6,6'-(terephthaloylbis(azanediyl))dihexanoic acid (392 mg, 1.00 mmol, 1 equiv) in DMF (10 mL) was added to a solution of EDC·HCl (767 mg, 4.00 mmol, 4 equiv) and DMAP (122 mg, 1.00 mmol, 1 equiv) in DMF (20 mL). The mixture was stirred for 2 h at 25 °C. Then, a solution of 6-amino-6-mono-deoxy- α -cyclodextrin⁶ (2.43 g, 2.50 mmol, 2.5 equiv) in DMF (30 mL) was added and the mixture stirred for further 3 d at 25 °C. The solution was poured into acetone (200 mL) under stirring, the precipitate was filtered off and washed with acetone. This crude product was dried *in vacuo* and purified by preparative HPLC. Yield: 483 mg (0.21 mmol, 21%, colourless solid); mp.: >250 °C; ^1H NMR (400 MHz, $\text{DMSO-}d_6$, 25 °C): δ = 8.56 (t, 3J = 5.5 Hz, 2H, NH), 7.89 (s, 4H, 16-H), 5.65-5.32 (m, 24H, 2-OH, 3-OH), 4.88-4.75 (m, 12H, 1/1'-H), 4.67-4.21 (m, 16H, 6-OH, NH, 7-H), 3.86-3.62 (m, 44H, 3/3'H, 5/5'H, 6-H), 3.39-3.32 (beneath HDO signal) (m, 12H, 4/4'-H), 3.31-3.14 (m, 16H, 2/2'-H, 13-H), 2.39-3.27 (m, 4H, 9-H), 1.64-1.47 (m, 8H, 10-H, 12-H), 1.39-1.27 (m, 4H, 11-H) ppm; ^{13}C NMR (151 MHz, $\text{DMSO-}d_6$, 25 °C): δ = 172.8 (8-C), 165.5 (14-C), 136.7 (15-C), 127.1 (16-C), 102.2-101.7 (m, 1/1'-C), 82.4-81.9 (m, 4/4'-C), 73.3-73.1 (m, 3/3'-C), 72.1-72.0 (m, 2/2'-C, 5-C), 68.9 (5'-C), 63.1 (7-C), 60.0-59.9 (m, 6-H), 38.9 (beneath $\text{DMSO-}d_6$ signal, from HSQC,

13-C), 33.3 (9-C), 28.8 (12-C), 26.0 (11-C), 24.2 (10-C) ppm; MS (ESI+) m/z (%): 1151.4 (100%) $[M+2H]^{2+}$; CHN calculated for $C_{92}H_{146}N_4O_{62} \cdot 14H_2O$ (M.W. 2552.34) C, 43.29; H, 6.87; N, 2.35; found C, 43.41; H, 6.67; N, 2.35.

Synthesis of b β CD



b β CD

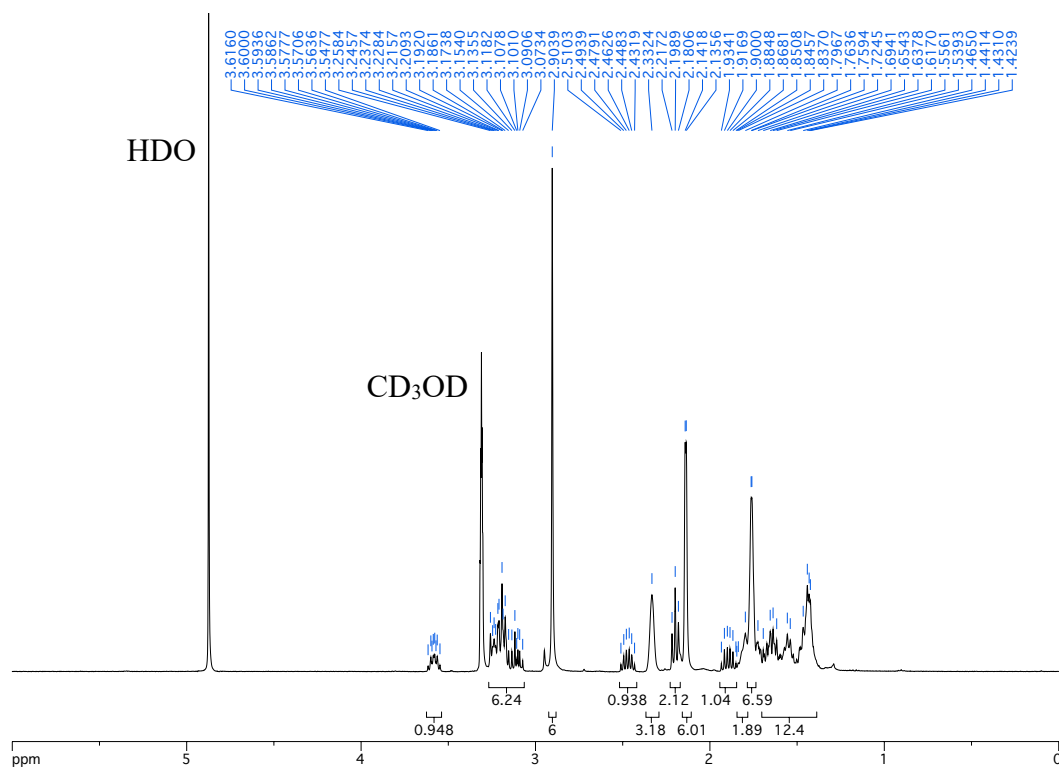


A solution of 6,6'-(terephthaloylbis(azanediyl))dihexanoic acid (570 mg, 1.45 mmol, 1 equiv) in DMF (20 mL) was added to a solution of EDC·HCl (1.11 g, 5.80 mmol, 4 eq.) and DMAP (177 mg, 1.45 mmol, 1 equiv) in DMF (25 mL). The mixture was stirred for 2 h at 25 °C. Then, a solution of 6-amino-6-mono-deoxy- β -cyclodextrin⁶ (4.11 g, 3.62 mmol, 2.5 equiv) in DMF (50 mL) was added and the mixture stirred for further 3 d at 25 °C. The solution was poured into acetone (300 mL) under stirring, the precipitate was filtered off and washed with acetone. This crude product was dried *in vacuo* and purified by preparative HPLC. Yield: 2.85 g (1.08 mmol, 75%, colourless solid); mp.: >250 °C; 1H NMR (400 MHz, DMSO- d_6 , 25 °C): δ = 8.55 (t, 3J = 5.1 Hz, 2H, NH), 7.89 (s, 4H, 18-H), 7.60 (sb, 2H, NH), 5.79-5.67 (m, 28H, 2-OH, 3-OH), 4.86-4.78 (m, 14H, 1/1'-H), 4.53-4.44 (m, 12H, 6-OH), 3.62-3.54 (m, 54H, 3/3'-H, 5/5'-H, 6-H, 7-H(2H)), 3.52-3.21 (beneath HDO signal) (m,

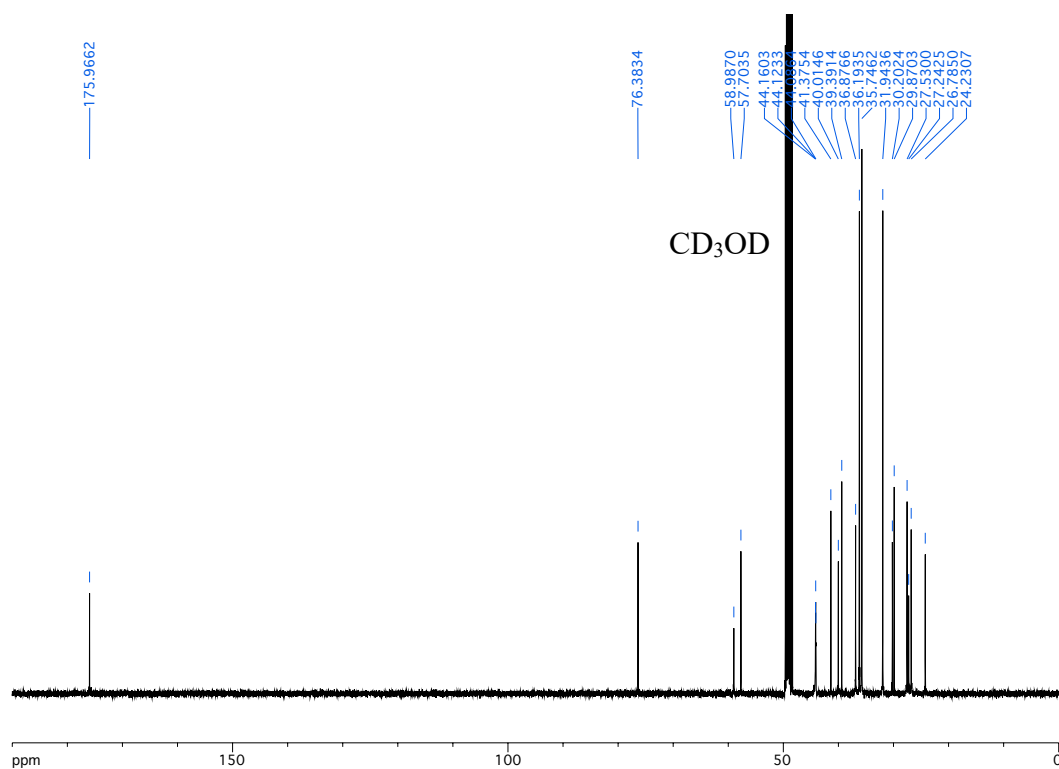
34H, 2/2'-H, 5/5'-H, 7-H(2H), 13-H), 2.16-2.06 (m, 4H, 9-H), 1.58-1.42 (m, 8H, 10-H/12-H), 1.35-1.21 (m, 4H, 11-H) ppm; ^{13}C NMR (101 MHz, DMSO- d_6 , 25 °C): δ = 172.5 (8-C), 165.6 (14-C), 136.8 (15-C), 127.1 (16-C), 102.3-101.8 (m, 1/1'-C), 83.7 (4'-C), 81.7-81.4 (m, 4-C), 73.2-72.9 (m, 3/3'-C), 72.5-72.4 (m, 2/2'-C), 72.2-72.0 (m, 5-C), 69.9 (5'-C), 60.1-59.8 (m, 6-C), 39.4 (beneath DMSO- d_6 signal, from HSQC, 13-C), 39.1 (beneath DMSO- d_6 signal, from HSQC, 7-C), 35.1 (9-C), 29.0 (12-C), 26.3 (11-C), 25.0 (10-C) ppm; MS (ESI+) m/z (%): 1312.5 (100%) $[\text{M}+2\text{H}]^{2+}$; CHN calculated for $\text{C}_{104}\text{H}_{166}\text{N}_4\text{O}_{72}\cdot 18\text{H}_2\text{O}$ (2948.68) C, 42.36; H, 6.90; N, 1.90; found C, 42.24; H, 6.69; N, 2.02.

NMR and Mass Spectra of LA

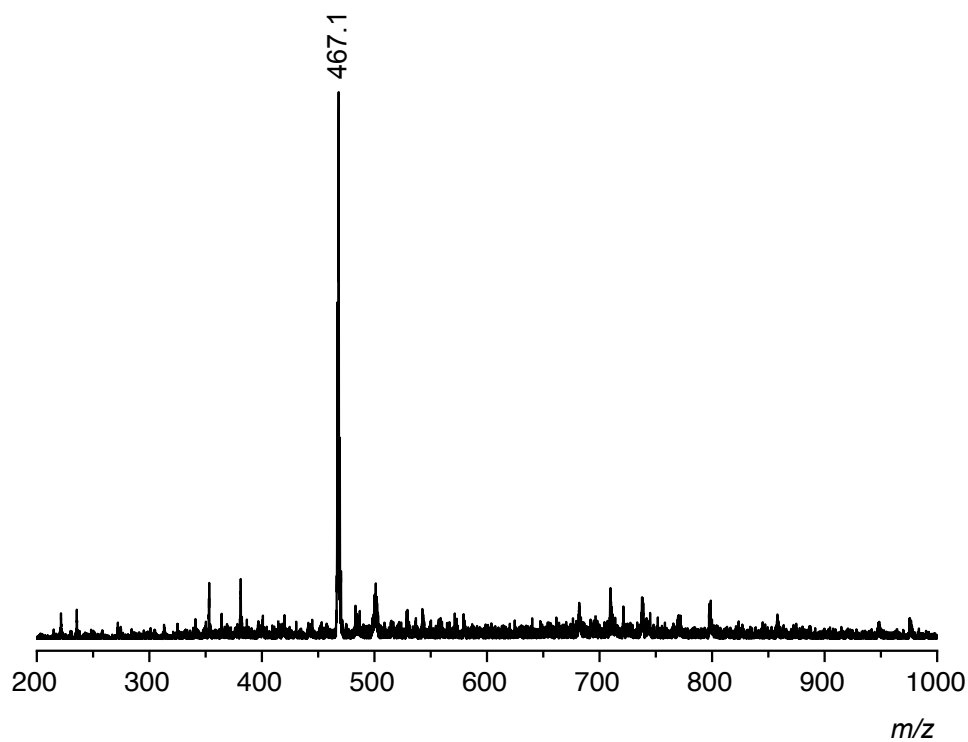
^1H NMR (400 MHz, CD_3OD)



^{13}C NMR (101 MHz, CD_3OD)

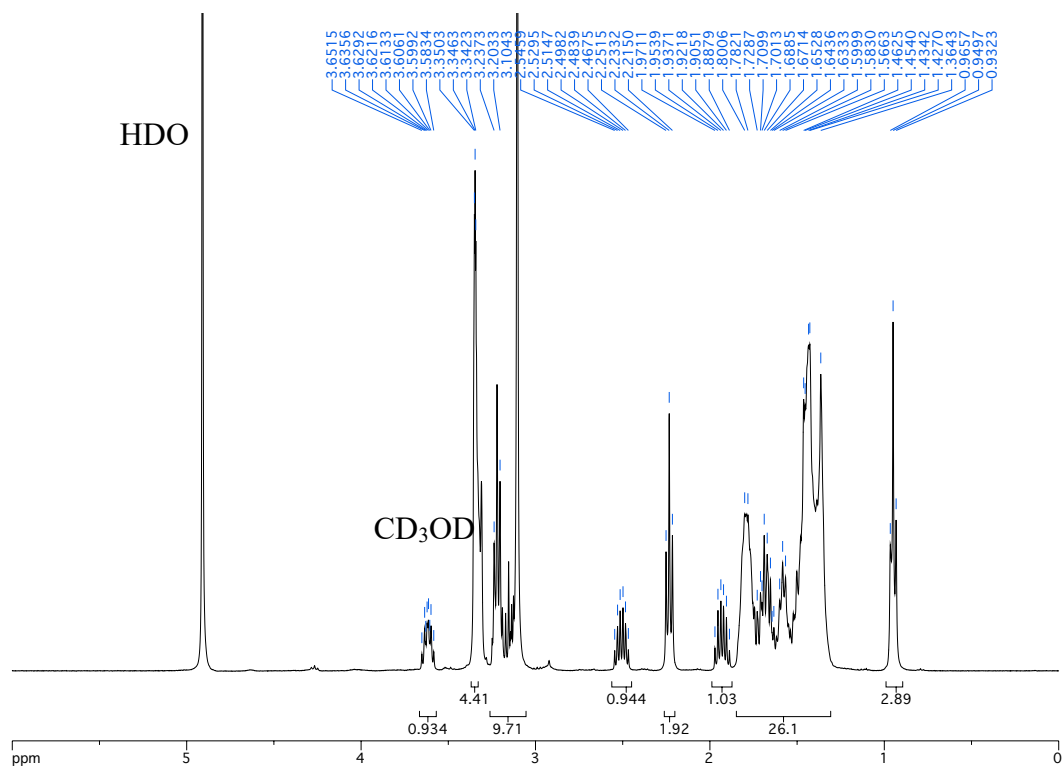
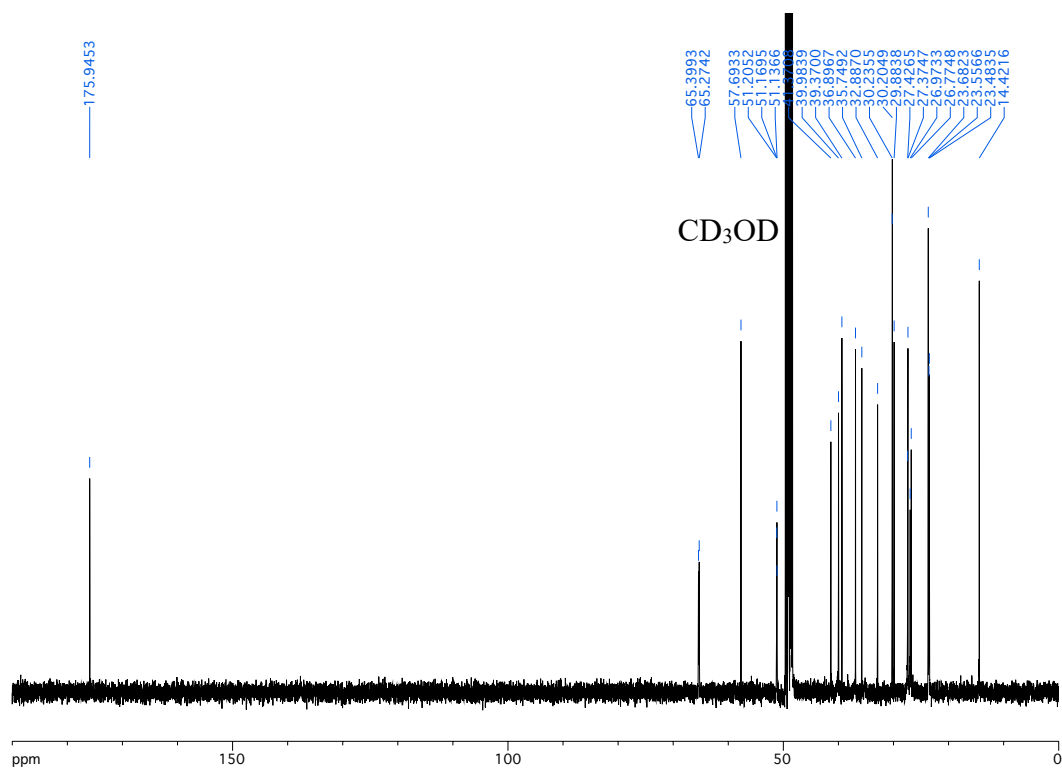


ESI-TOF MS (positive mode)

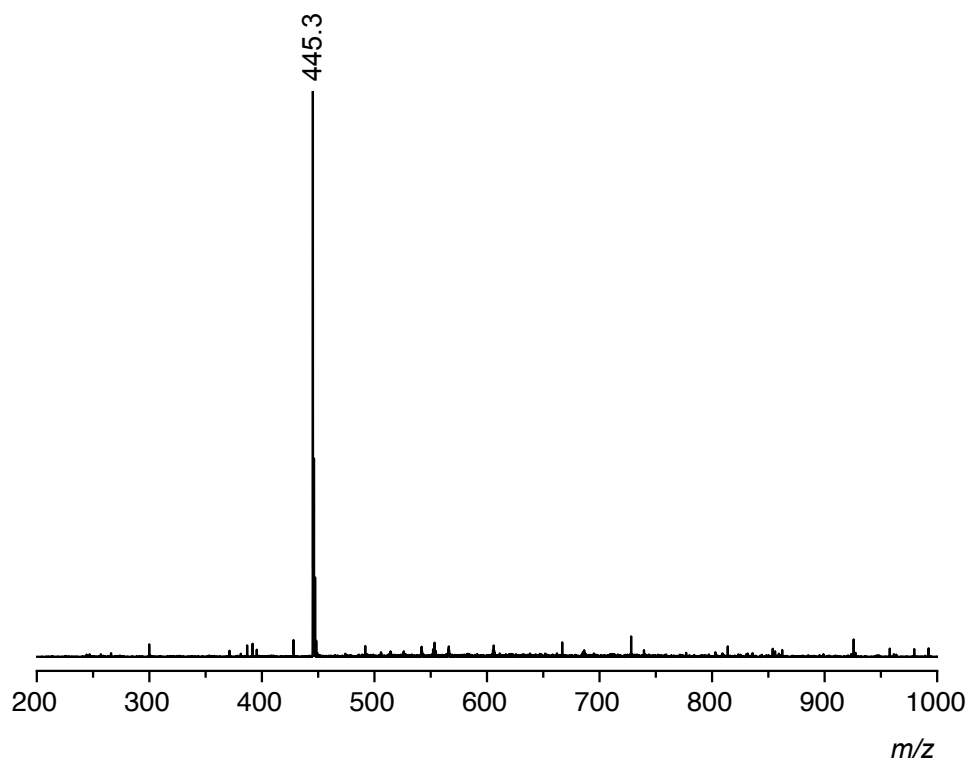


		<i>m/z calcd.</i>	<i>m/z exp.</i>
$[M-Br]^+$	$C_{26}H_{47}N_2OS_2^+$	467.3	467.1

NMR and Mass Spectra of LO

¹H NMR (400 MHz, CD₃OD)¹³C NMR (101 MHz, CD₃OD)

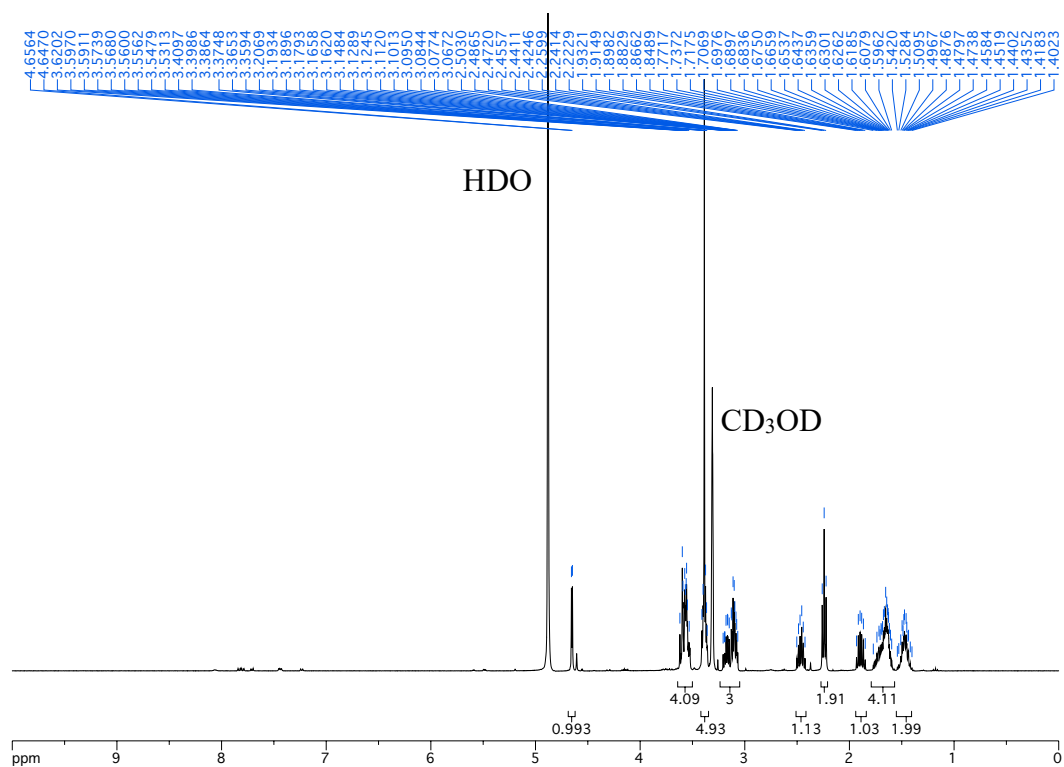
ESI-TOF MS (positive mode)



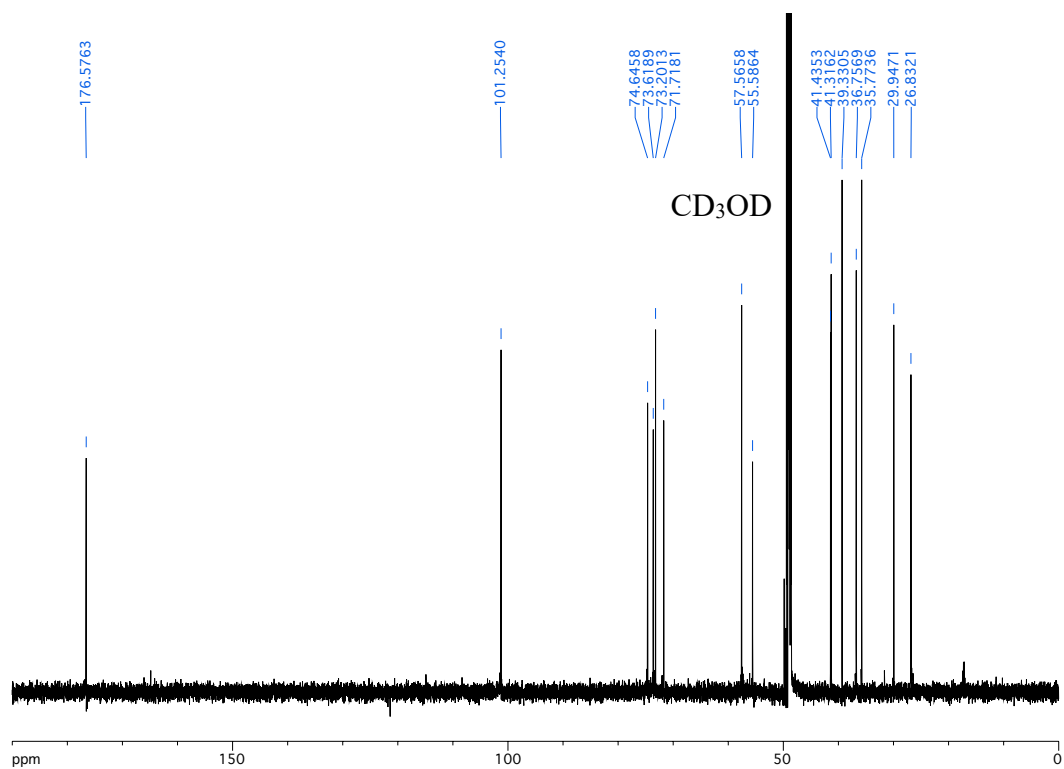
		<i>m/z calcd.</i>	<i>m/z exp.</i>
$[M-Br]^+$	$C_{24}H_{49}N_2OS_2^+$	445.3	445.3

NMR and Mass Spectra of LG

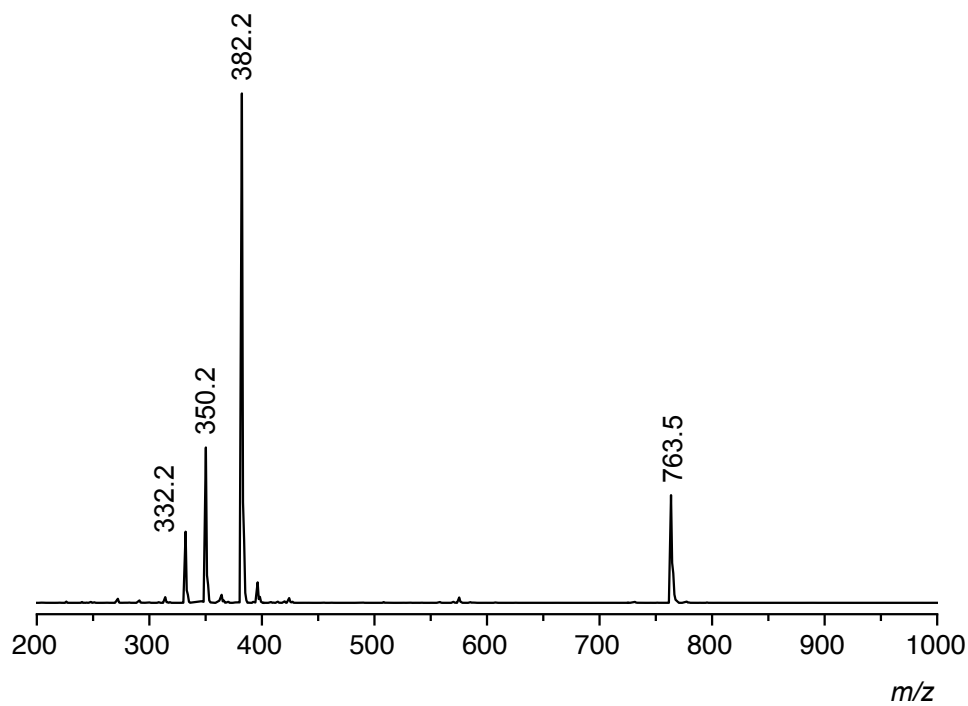
^1H NMR (400 MHz, CD_3OD)



^{13}C NMR (101 MHz, CD_3OD)



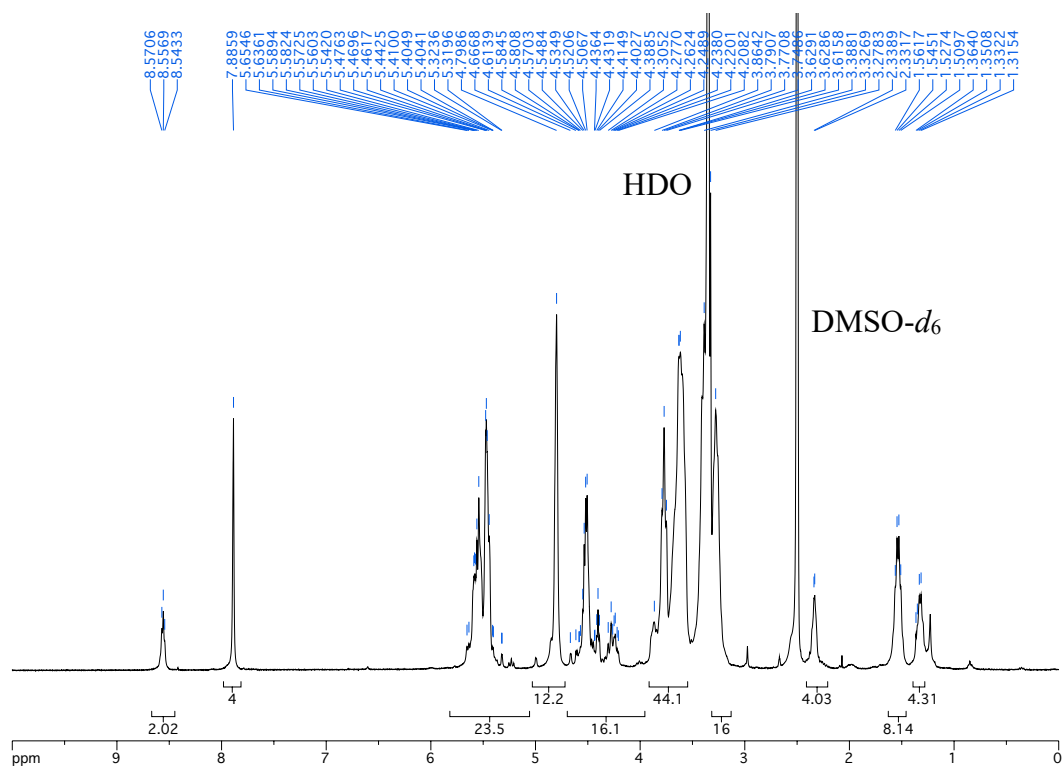
ESI-TOF MS (positive mode)



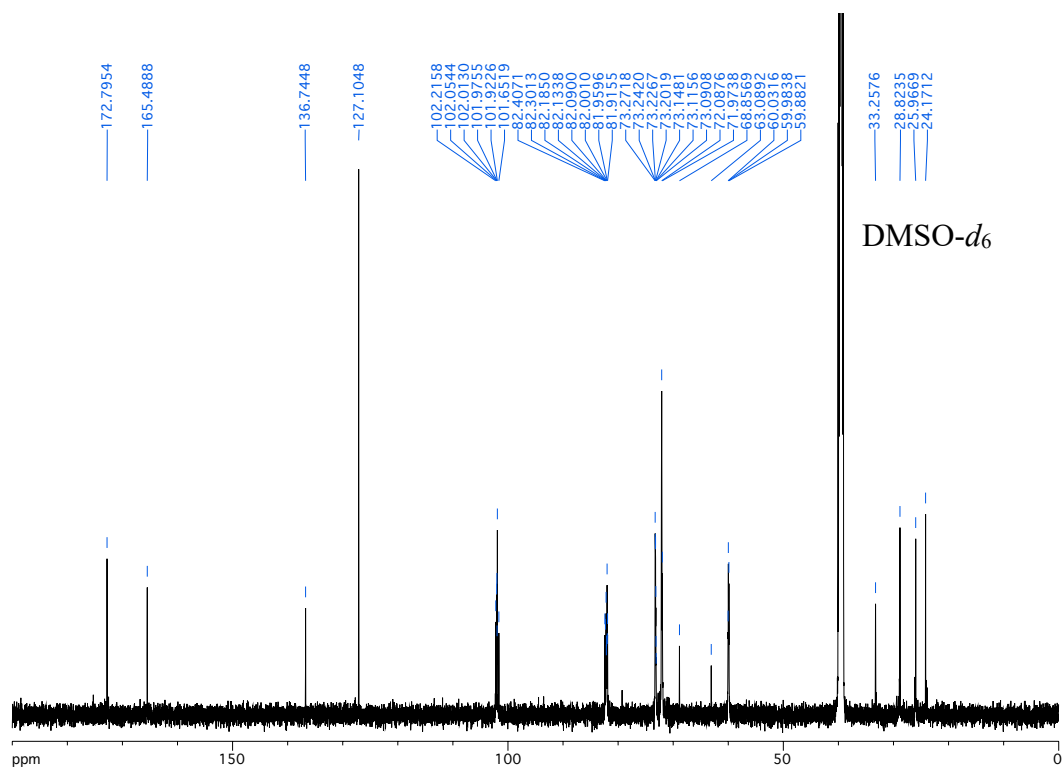
		m/z calcd.	m/z exp.
$[M-CH_3OH-H_2O+H]^+$	$C_{15}H_{27}NO_6S_2$	332.1	332.2
$[M-CH_3OH+H]^+$	$C_{14}H_{24}NO_5S_2^+$	350.1	350.2
$[M+H]^+$	$C_{15}H_{28}NO_6S_2^+$	382.1	382.2
$[M_2+H]^+$	$(C_{15}H_{27}NO_6S_2)(C_{15}H_{28}NO_6S_2)^+$	763.3	763.5

NMR Spectra, Mass Spectra, and HPLC Chromatogram of β CD

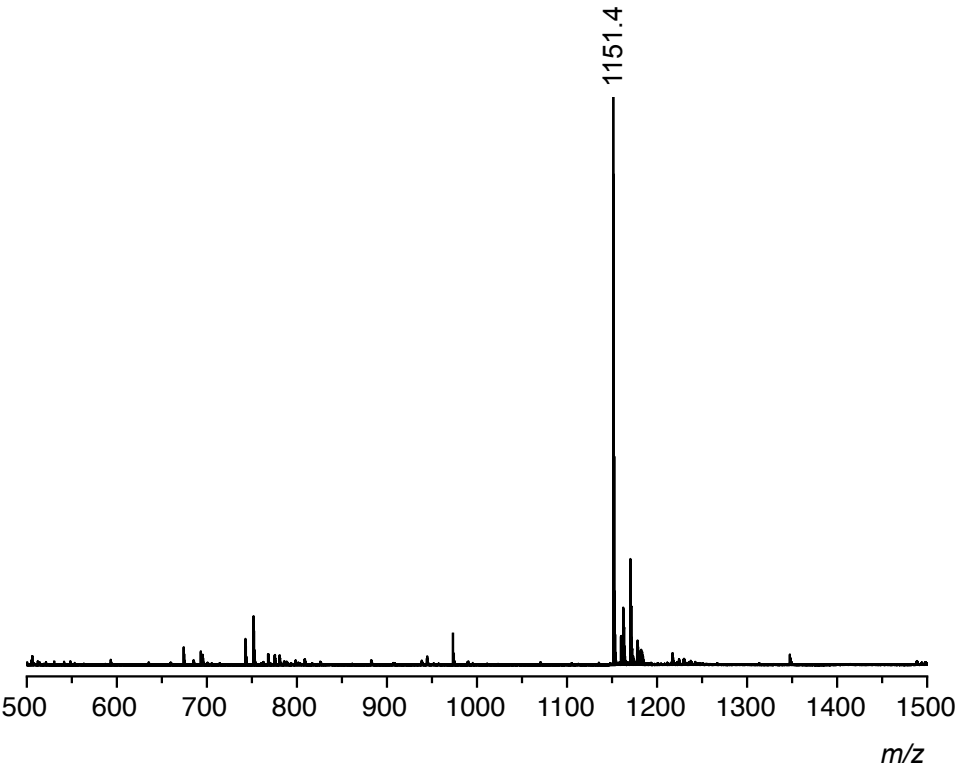
^1H NMR (600 MHz, $\text{DMSO-}d_6$)



^{13}C NMR (151 MHz, $\text{DMSO-}d_6$)

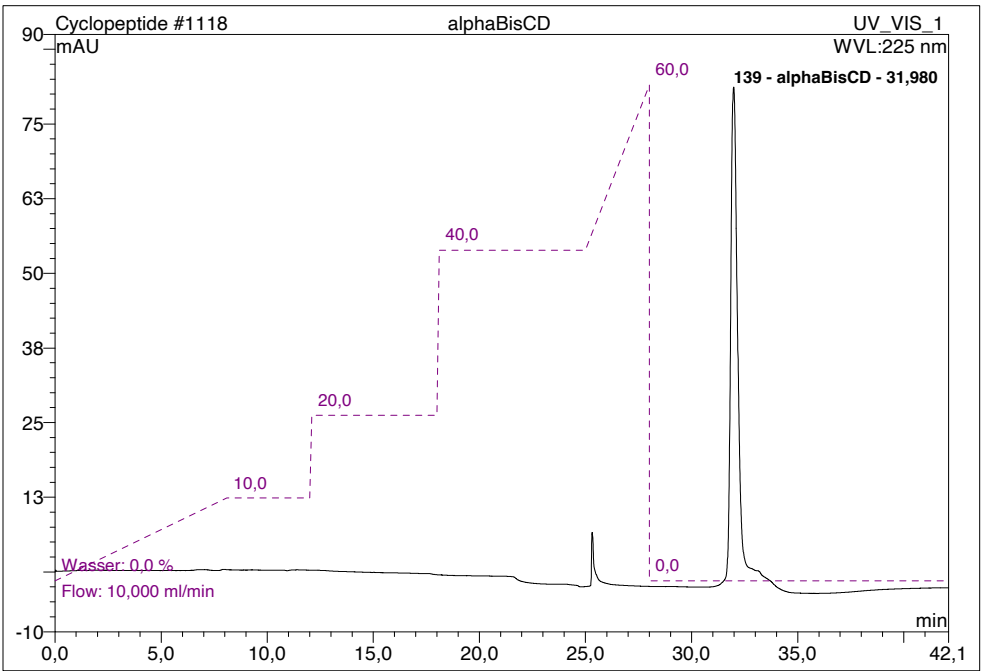


ESI-TOF MS (positive mode)



		<i>m/z calcd.</i>	<i>m/z exp.</i>
$[M+2H]^{2+}$	$C_{92}H_{148}N_4O_{62}^{2+}$	1150.9	1151.4

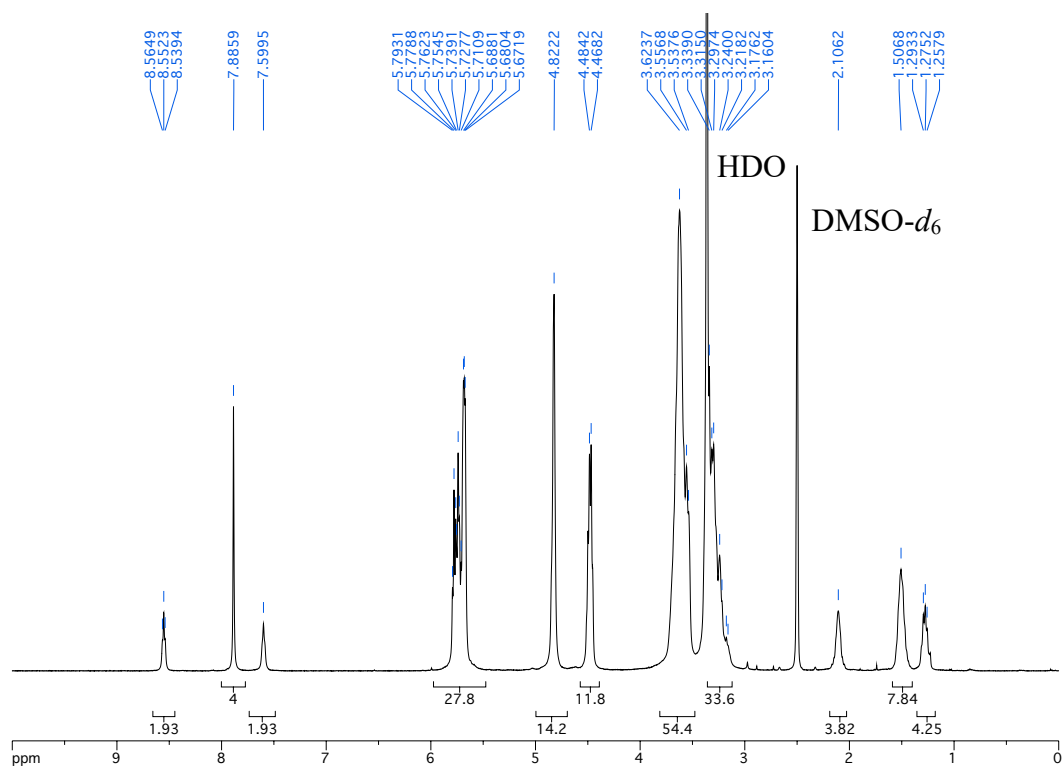
1118 alphaBisCD			
Sample Name:	alphaBisCD	Injection Volume:	500,0
Vial Number:	GE1	Channel:	UV_VIS_1
Sample Type:	unknown	Wavelength:	225
Control Program:	StufenBisCD2	Bandwidth:	n.a.
Quantif. Method:	default	Dilution Factor:	1,0000
Recording Time:	25.2.2025 10:48	Sample Weight:	1,0000
Run Time (min):	42,10	Sample Amount:	1,0000



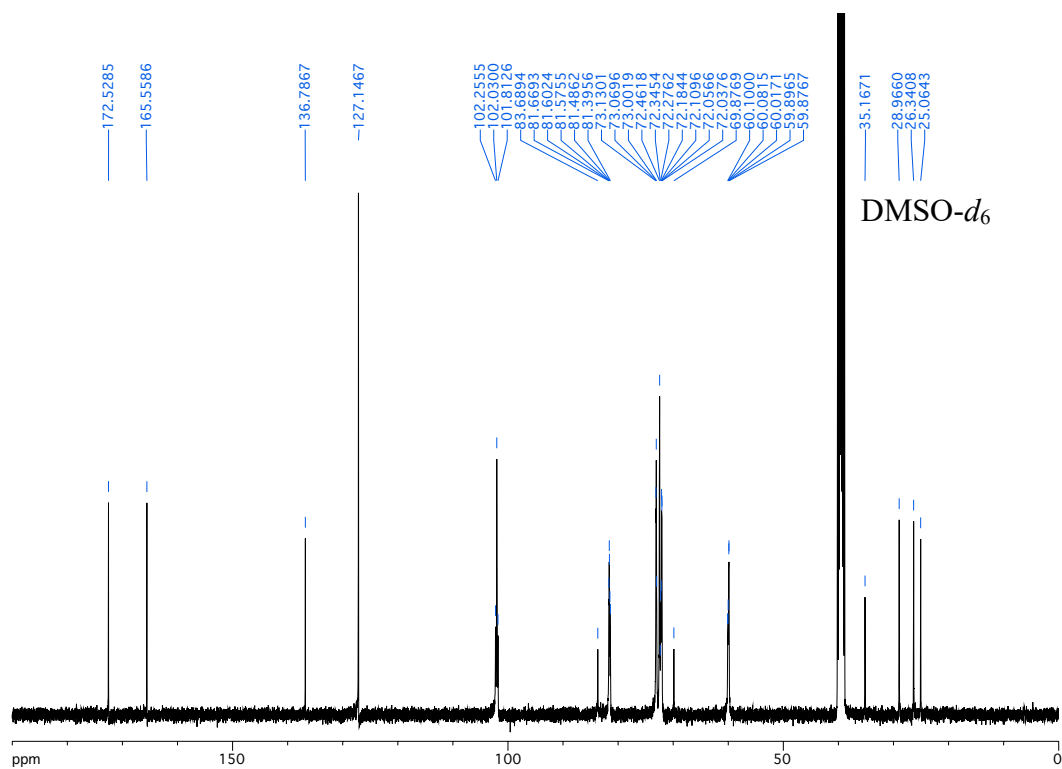
No.	Ret.Time min	Peak Name	Height mAU	Area mAU*min	Rel.Area %	Amount	Type
139	31,98	alphaBisCD	82,442	30,471	92,76	n.a.	BM
Total:			82,442	30,471	92,76	0,000	

NMR Spectra, Mass Spectra, and HPLC Chromatogram of b β CD

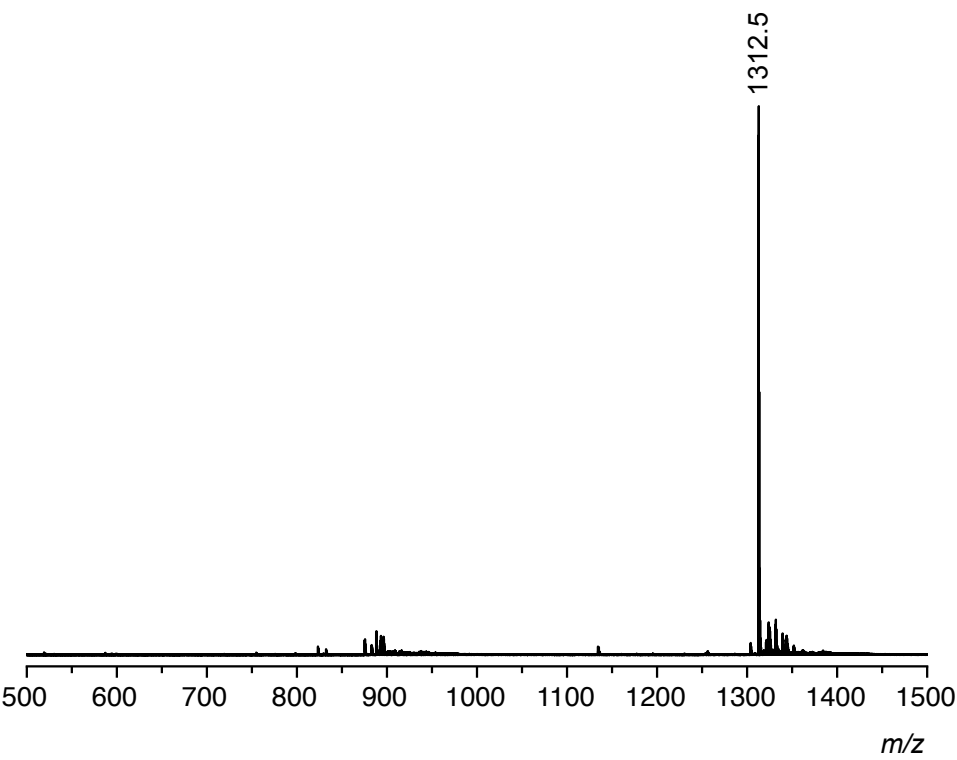
^1H NMR (400 MHz, $\text{DMSO-}d_6$)



^{13}C NMR (101 MHz, $\text{DMSO-}d_6$)

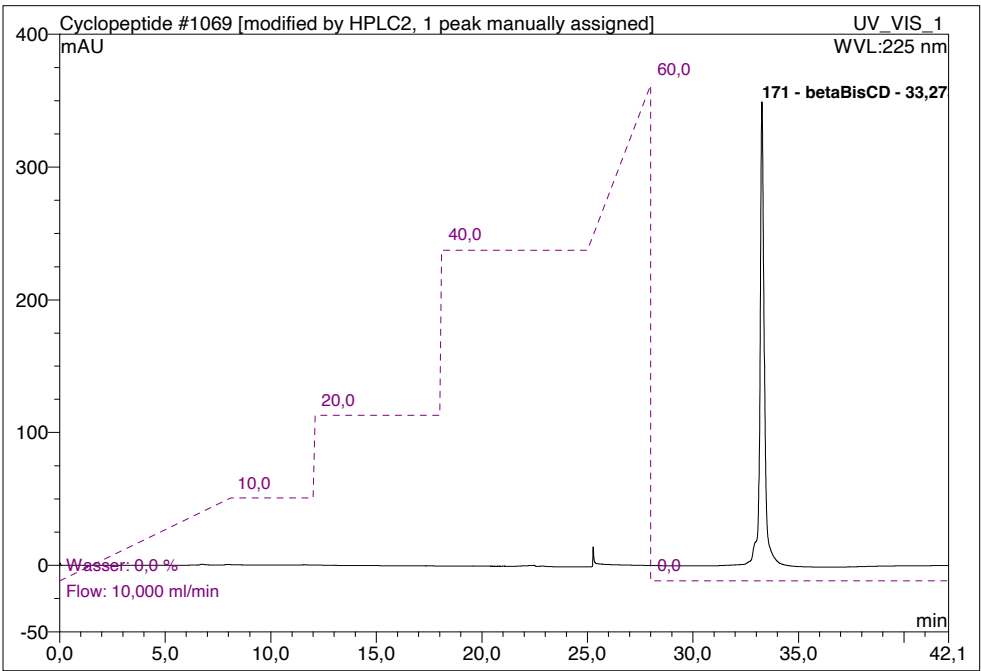


ESI-TOF MS (positive mode)



		<i>m/z calcd.</i>	<i>m/z exp.</i>
$[M+2H]^{2+}$	$C_{104}H_{168}N_4O_{72}^{2+}$	1313.0	1312.5

1069 beta			
Sample Name:	beta	Injection Volume:	500,0
Vial Number:	GA1	Channel:	UV_VIS_1
Sample Type:	unknown	Wavelength:	225
Control Program:	StufenBisCD2	Bandwidth:	n.a.
Quantif. Method:	default	Dilution Factor:	1,0000
Recording Time:	3.2.2025 9:08	Sample Weight:	1,0000
Run Time (min):	42,10	Sample Amount:	1,0000



No.	Ret.Time min	Peak Name	Height mAU	Area mAU*min	Rel.Area %	Amount	Type
171	33,27	betaBisCD	349,555	86,069	94,66	n.a.	MB*^
Total:			349,555	86,069	94,66	0,000	

ITC and NMR titrations

ITC Titrations. The solvents used in the ITC titrations were of HPLC grade. Receptors and guests were weighed using an analytical precision balance, dissolved in known volumes of the solvent and loaded into the system for immediate analysis. Solutions involved in the same titration experiment were made up from the same batch of solvent. The concentrations of the receptors and substrates are summarized in Table S1. A standard ITC experiment involved the titration of a solution of the salt or ligand into a solution of the receptor at 25 °C by using 30 injections of 8 μ L, separated by an interval of 180 s, with the exception of the first injection, which was 4 μ L. Binding constants and enthalpies of binding were obtained by curve fitting of the titration data using the 1:1 binding model for the α CD and β CD complexes and the noncooperative 2:1 binding model for the bis(cyclodextrins) **b α CD** and **b β CD** as implemented in SupraFit.⁷ The titrations were performed at least three times and the log K_a value given below are the means of the result of the individual measurements.

Table S1: Concentrations of cyclodextrins and salt solutions used in the ITC measurements.

Receptor	Salt	$c(\text{Receptor})$ / mM	$c(\text{Salt})$ / mM
α CD	TMOI	0.50	10
α CD	TMAI	0.50	10
α CD	LA	2	40
β CD	TMOI	2	40
β CD	TMAI	0.50	10
β CD	LA	0.50	10
bαCD	TMOI	0.50	10
bβCD	TMOI	1	20
bαCD	TMAI	1	20
bβCD	TMAI	0.25	5

NMR Titrations. The titration was performed on a Bruker Avance™ III 400 spectrometer (400 MHz) with 128 scans and 25 °C. D₂O was used as purchased. The receptors and salts were weighed using an analytical precision balance and used to prepare stock solutions in D₂O. For titrations with β CD, the concentrations of both stock solutions were 10 mM, while they were 20 mM for titrations with α CD. Dimethyl sulfone (DMS) was used as reference, which was added as a 10 mM stock solution in D₂O. Eighteen NMR tubes were prepared, each containing 50 μ L of the stock solution of the salt and

50 μL of the DMS solution. No receptor solution was added to the first NMR tube. To each of the other tubes different volumes of the receptor solution were added as specified in Table S2. The total volume in each NMR tube was made up to 500 μL , the samples were thoroughly shaken, and their spectra were recorded. In this way, the concentration of the salt was maintained at 1 mM throughout the titrations when using the 10 mM receptor solution, whereas the concentration of receptor varied between 0 and 5 mM. The concentrations were twice that high when the receptor stock solution had a concentration of 20 mM. The changes in the chemical shifts of selected guest protons were monitored and used to generate binding isotherms that were globally fitted to a 1:1 complex equilibrium by using a routine implemented in SupraFit.⁷

Table S2: Volumes of salt, reference, and receptor stock solutions used in the NMR titrations. The resulting concentrations are given when the stock solutions had concentrations of 10 mM. The receptor and salt concentrations in each sample were twice that high when 20 mM stock solutions were used.

#	$V(\text{Salt}) /$ μL	$V(\text{DMS})$ $/ \mu\text{L}$	$V(\text{Receptor})$ $/ \mu\text{L}$	$V(\text{D}_2\text{O})$ $/ \mu\text{L}$	$c(\text{Salt}) /$ mM	$c(\text{Receptor})$ $/ \text{mM}$
1	50	50	0	400	1.00	0
2	50	50	12.6	387	1.00	0.25
3	50	50	15	385	1.00	0.30
4	50	50	25	375	1.00	0.50
5	50	50	37.6	362	1.00	0.75
6	50	50	50	350	1.00	1.00
7	50	50	62.6	337	1.00	1.25
8	50	50	75	325	1.00	1.50
9	50	50	87.6	312	1.00	1.75
10	50	50	100	300	1.00	2.00
11	50	50	112.6	287	1.00	2.25
12	50	50	125	275	1.00	2.50
13	50	50	137.6	262	1.00	2.75
14	50	50	150	250	1.00	3.00
15	50	50	175	225	1.00	3.50
16	50	50	200	200	1.00	4.00
17	50	50	225	175	1.00	4.50
18	50	50	250	150	1.00	5.00

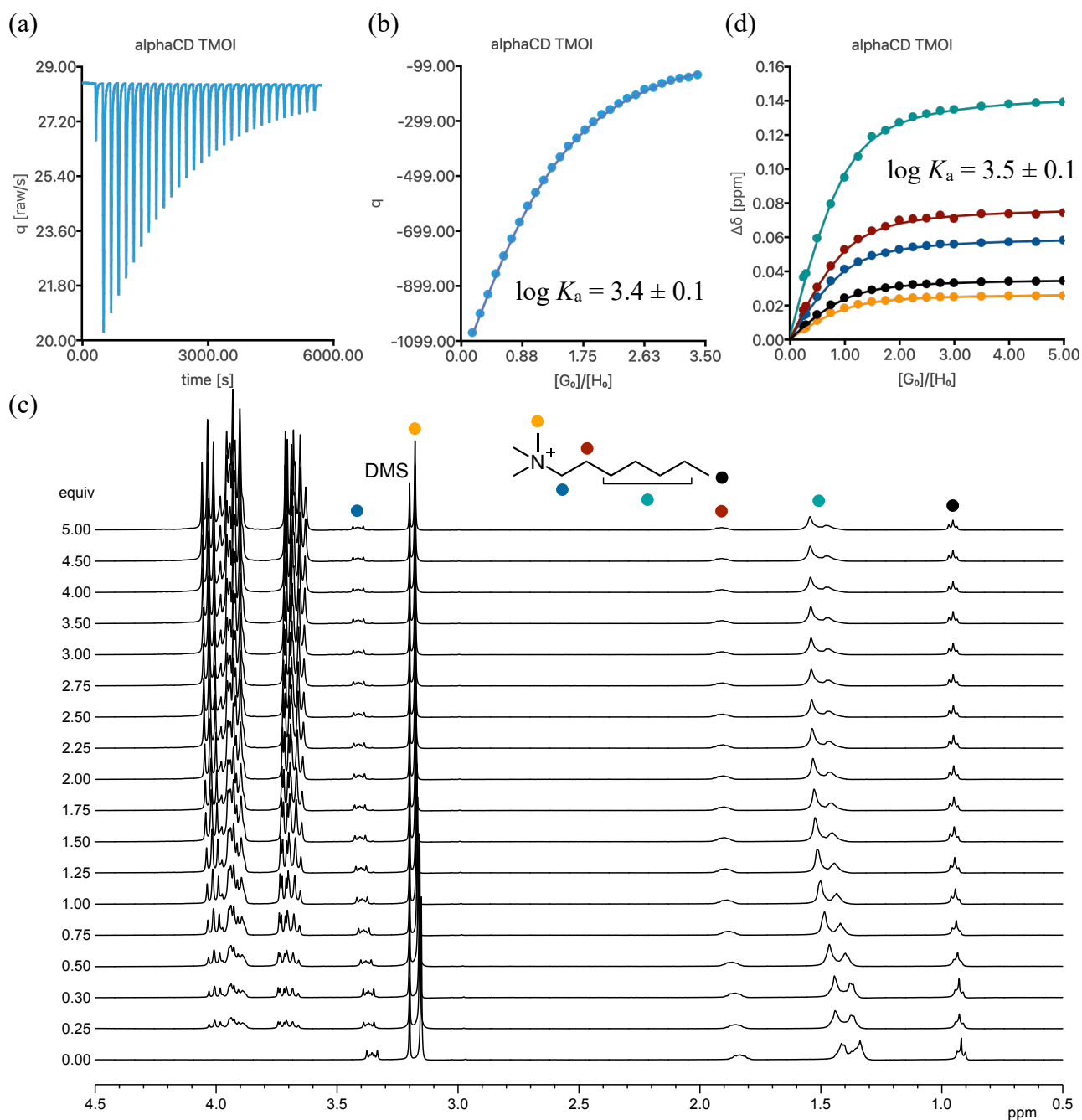


Figure S1: Thermogram (a) and binding isotherm (b) of the ITC titration of α CD with **TMOI**. The data points in the isotherms are the experimental values and the line shows the fit of the data to the 1:1 binding model. The spectra in (c) show the complexation-induced shifts of the guest signals followed in the ^1H NMR titration, and the plot in (d) the corresponding isotherms, with the circles and lines showing the experimental data and calculated isotherms resulting from global fitting, respectively.

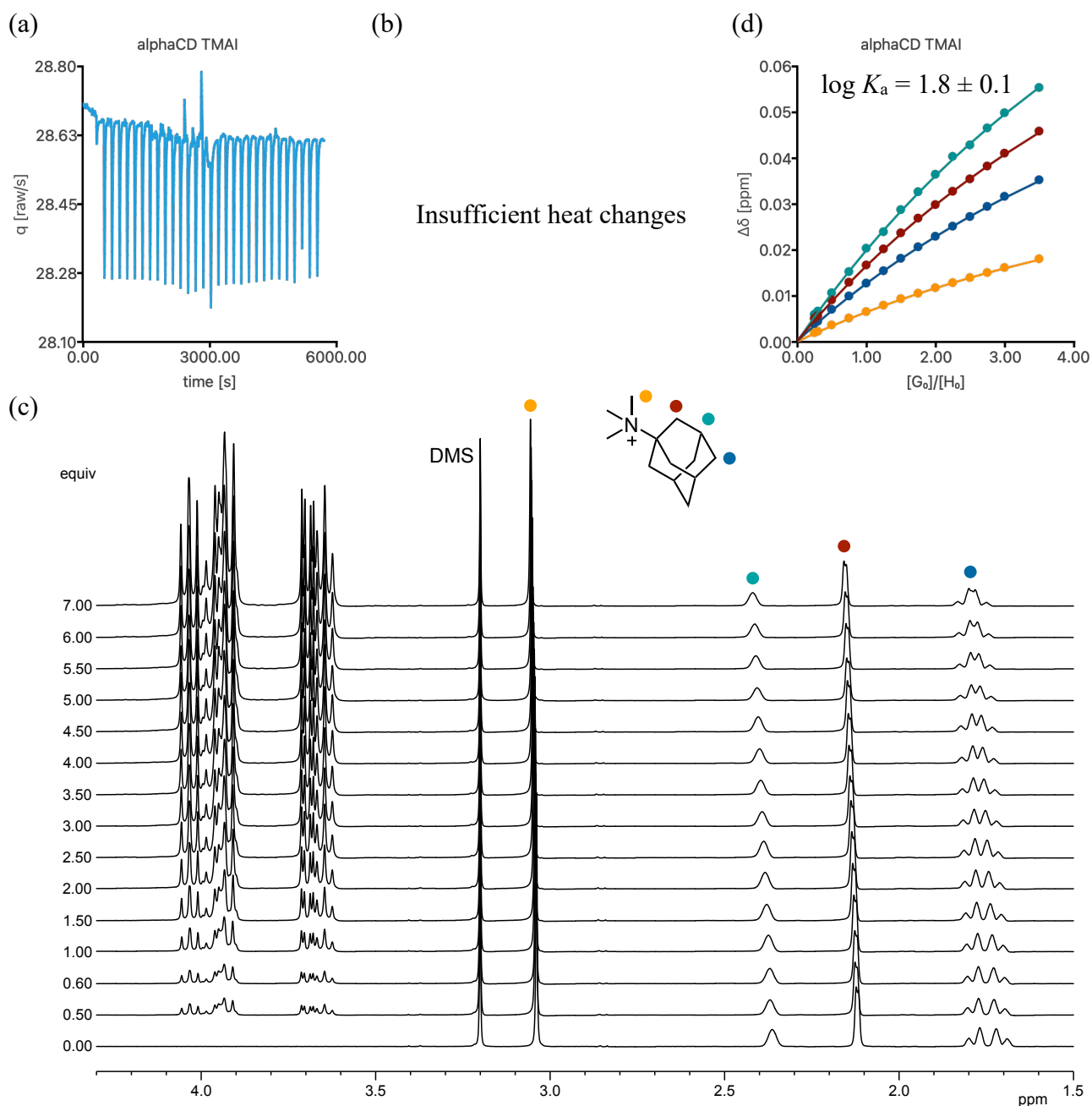


Figure S2: Thermogram (a) of the ITC titration of α CD with **TMAI**. Due to the small heat pulses, the binding isotherm in (b) could not be obtained. The spectra in (c) show the complexation-induced shifts of the guest signals followed in the ^1H NMR titration, and the plot in (d) the corresponding isotherms, with the circles and lines showing the experimental data and calculated isotherms resulting from global fitting, respectively.

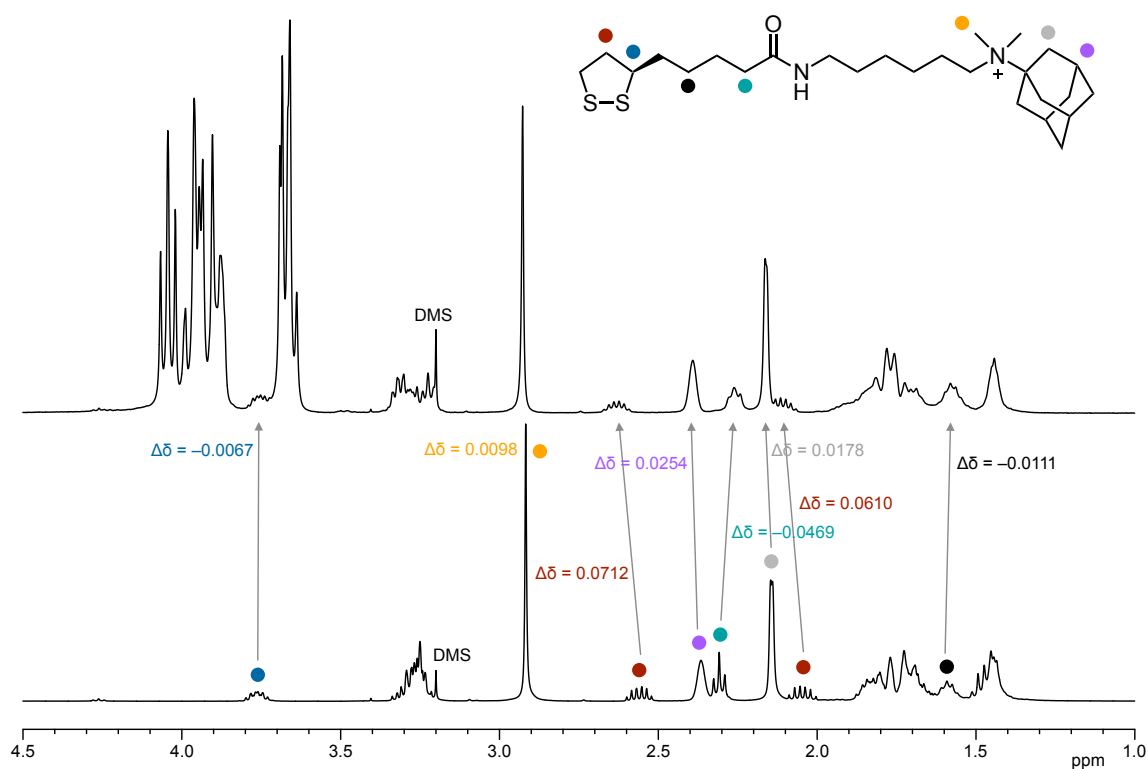


Figure S3: ^1H NMR spectra of **LA** (3.3 mM) in the absence and the presence of 2 molar equivalents of αCD in D_2O . The complexation-induced signal shifts indicate that the cyclodextrin interacts with both parts of **LA**.

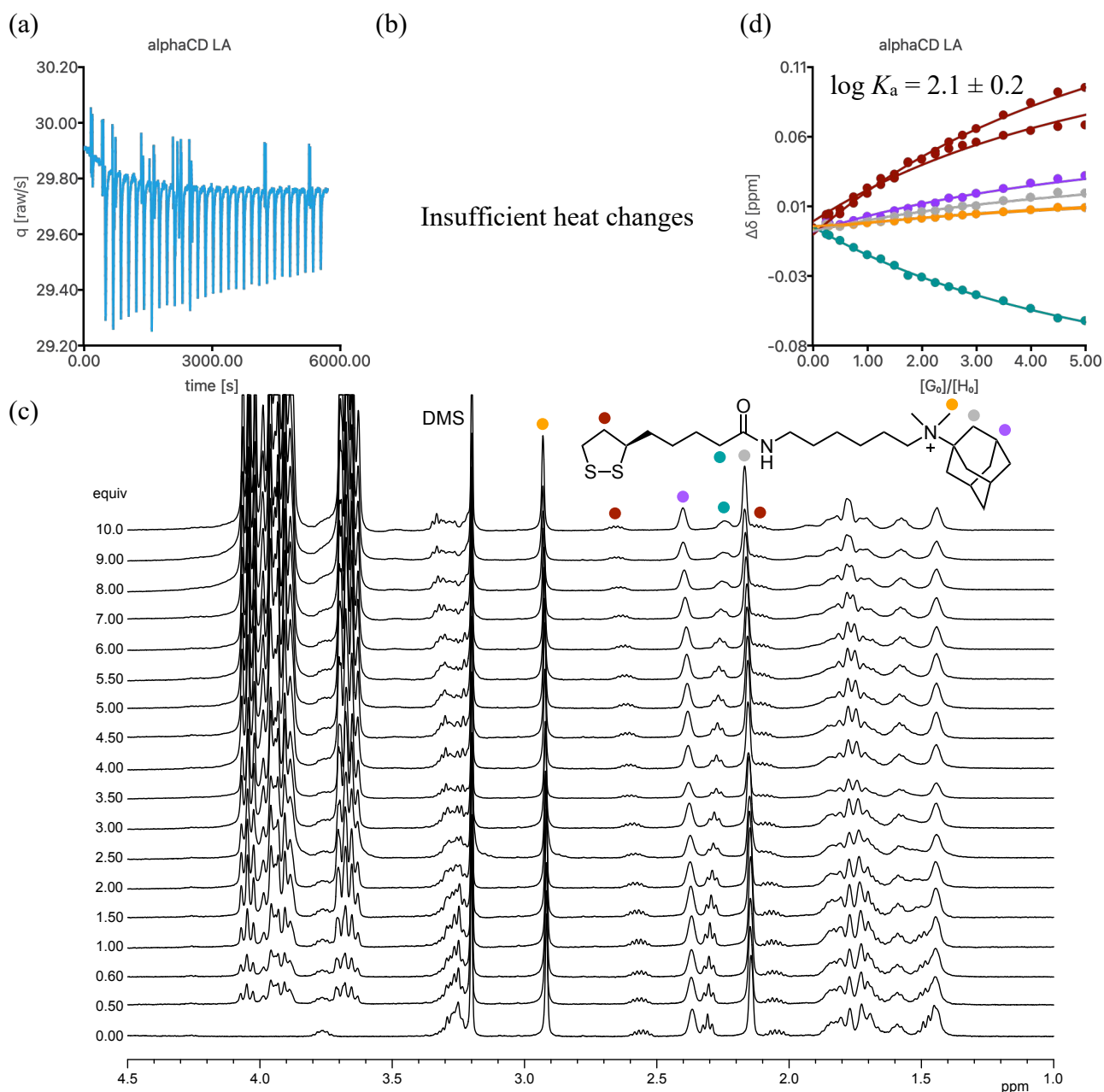


Figure S4: Thermogram (a) and binding isotherm (b) of the ITC titration of α CD with LA. Due to the small heat pulses, the binding isotherm in (b) could not be obtained. Therefore, an NMR titration was performed. The spectra in (c) show the complexation-induced shifts of the guest signals followed in the ^1H NMR titration, and the plot in (d) the corresponding isotherms, with the circles and lines showing the experimental data and calculated isotherms resulting from global fitting, respectively.

Deviations in one of the binding isotherms indicate that higher complexes could be present in this case, for example complexes with two α CD rings interacting with both ends of LA, which furthermore supports the statement in the manuscript that the ligands themselves are not ideal for the binding studies.

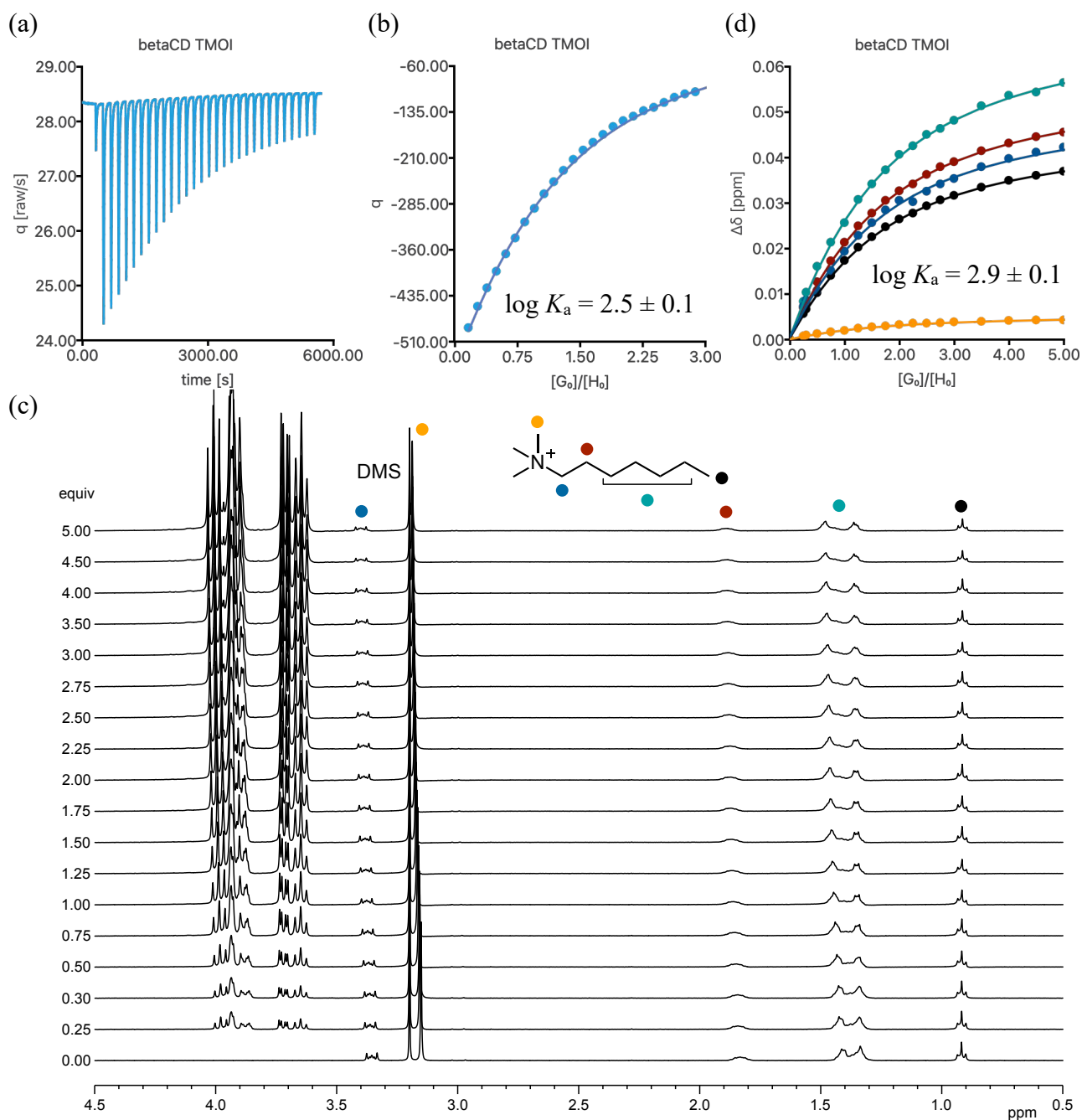


Figure S5: Thermogram (a) and binding isotherm (b) of the ITC titration of β CD with **TMOI**. The data points in the isotherms are the experimental values and the line shows the fit of the data to the 1:1 binding model. The spectra in (c) show the complexation-induced shifts of the guest signals followed in the ^1H NMR titration, and the plot in (d) the corresponding isotherms, with the circles and lines showing the experimental data and calculated isotherms resulting from global fitting, respectively.

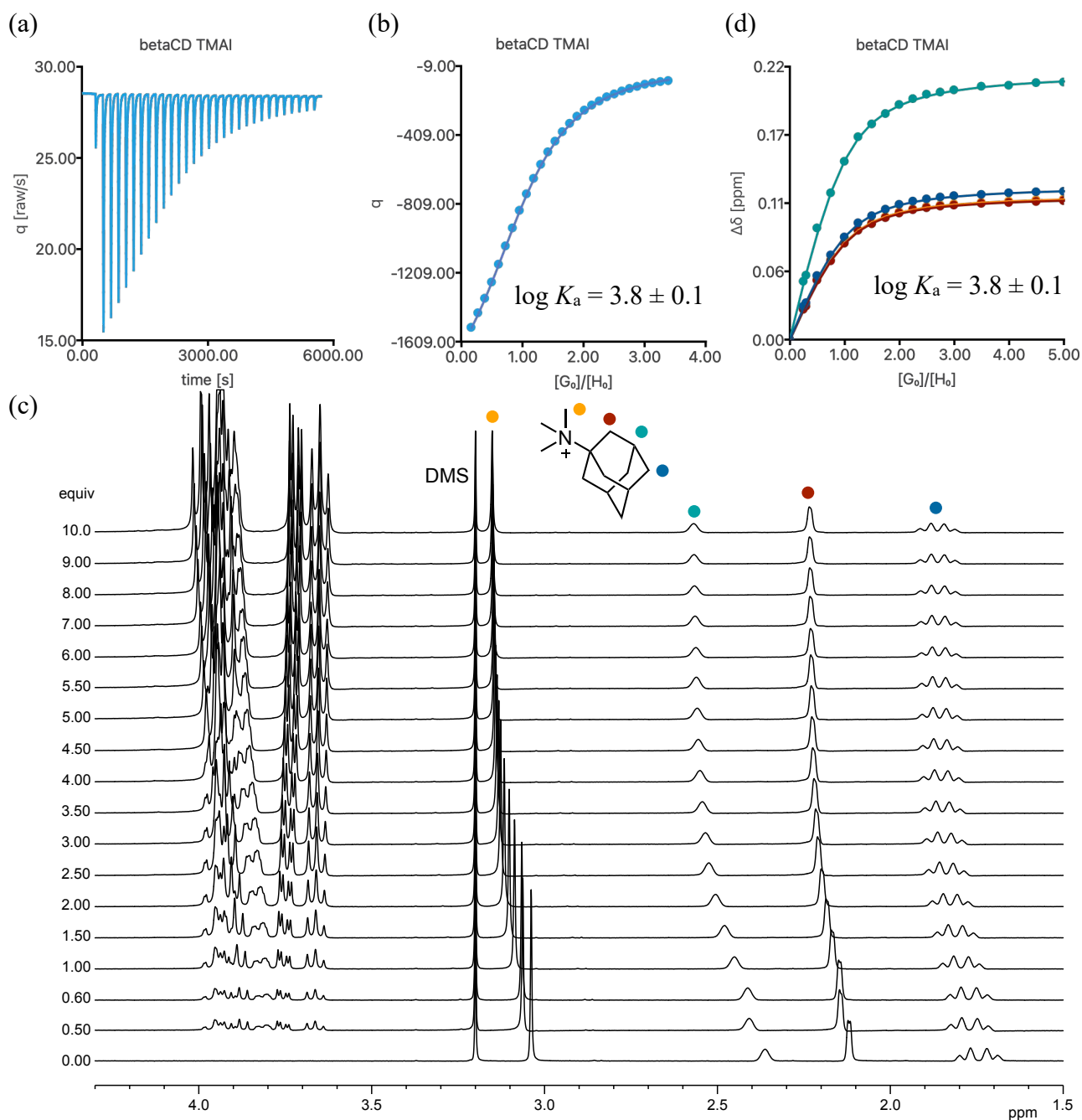


Figure S6: Thermogram (a) and binding isotherm (b) of the ITC titration of β CD with TMAI. The data points in the isotherms are the experimental values and the line shows the fit of the data to the 1:1 binding model. The spectra in (c) show the complexation-induced shifts of the guest signals followed in the ^1H NMR titration, and the plot in (d) the corresponding isotherms, with the circles and lines showing the experimental data and calculated isotherms resulting from global fitting, respectively.

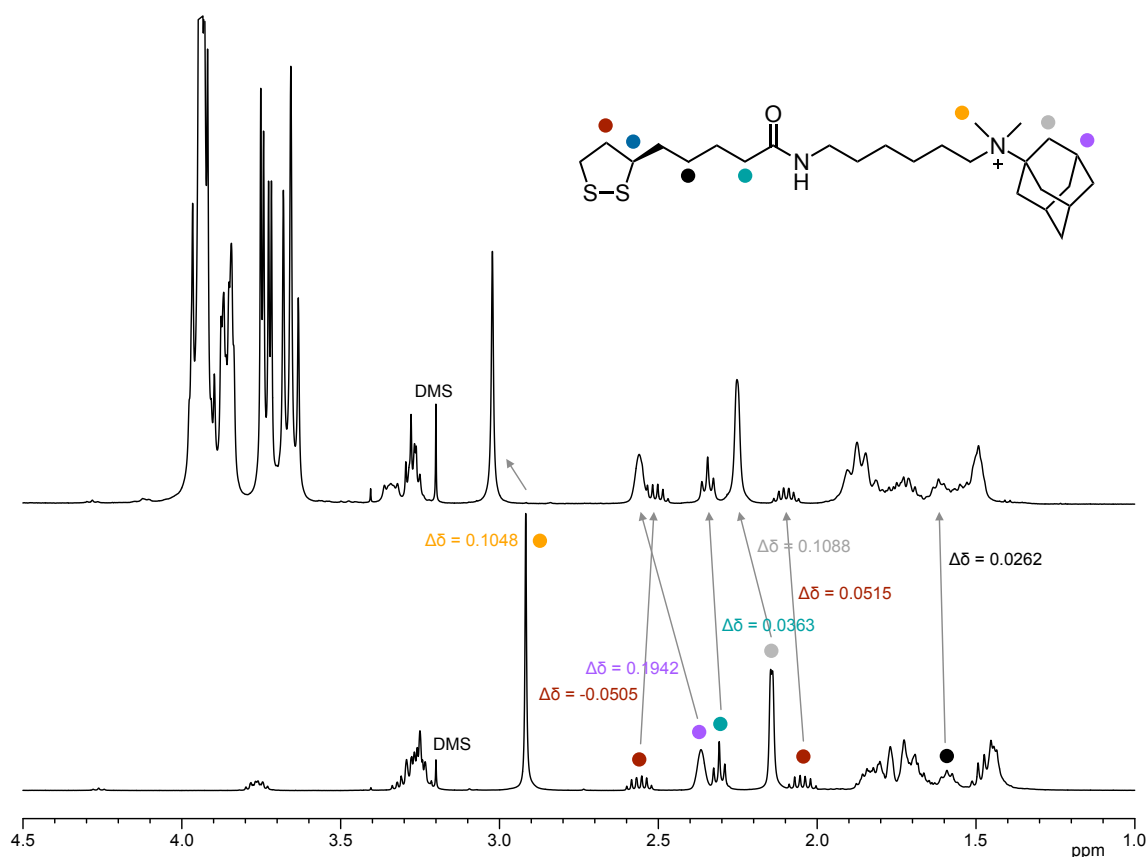


Figure S7: ^1H NMR spectra of **LA** (3.3 mM) in the absence and the presence of 2 molar equivalents of βCD in D_2O . The complexation-induced signal shifts indicate that the cyclodextrin interacts preferentially with the adamantyl residue of **LA**, as supported by the comparable $\log K_a$ values of the βCD complexes of **TMAI** and **LA** (Figure S6 and Figure S8).

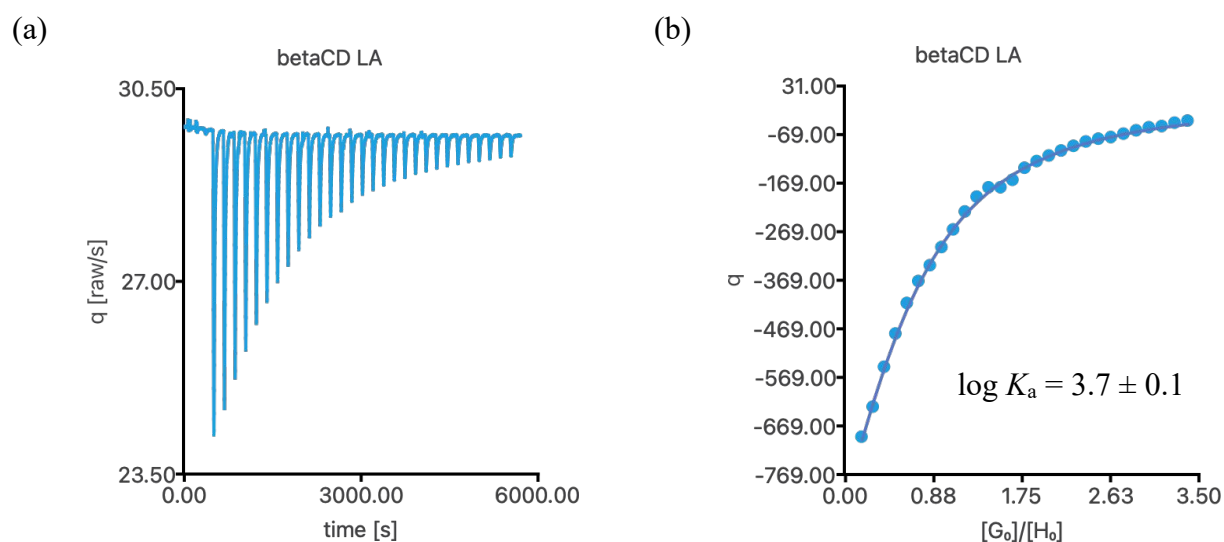


Figure S8: Thermogram (a) and binding isotherm (b) of the ITC titration of βCD with **LA**. The data points in the isotherms are the experimental values and the line shows the fit of the data to the 1:1 binding model.

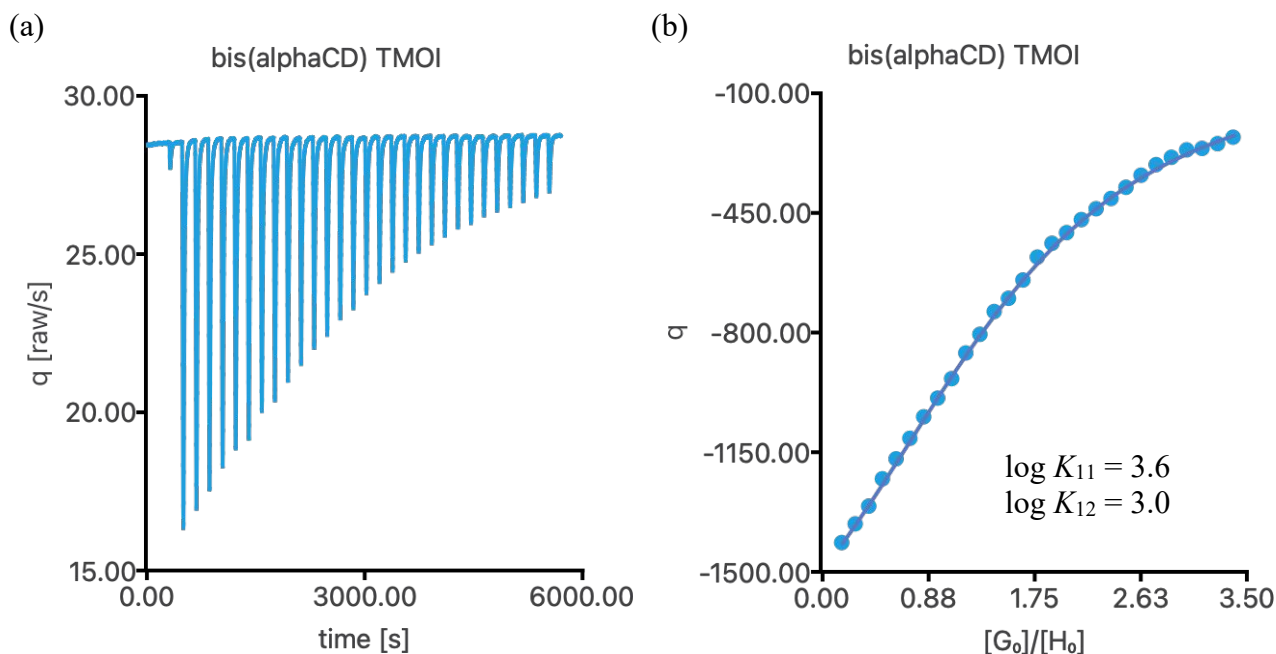


Figure S9: Thermogram (a) and binding isotherm (b) of the ITC titration of **baCD** with **TMOI**. The data points in the isotherms are the experimental values and the line shows the fit of the data to the noncooperative 1:2 binding model.

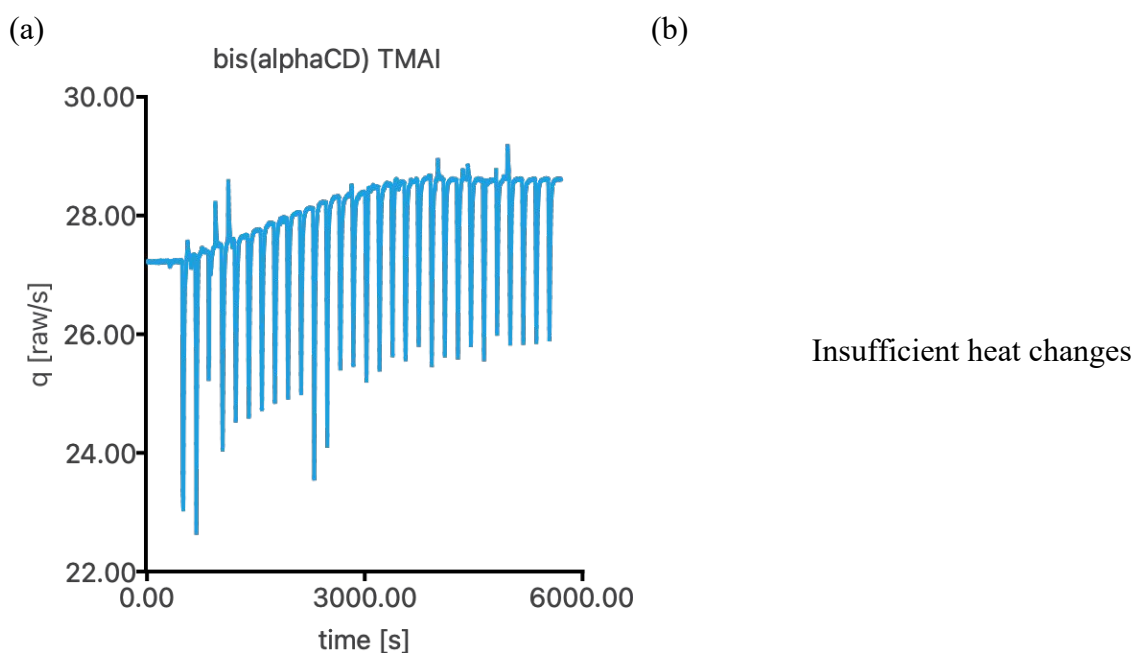


Figure S10: Thermogram (a) and binding isotherm (b) of the ITC titration of **baCD** with **TMAI**. Due to the scattering of the heat pulses, the binding isotherm in (b) could not be obtained.

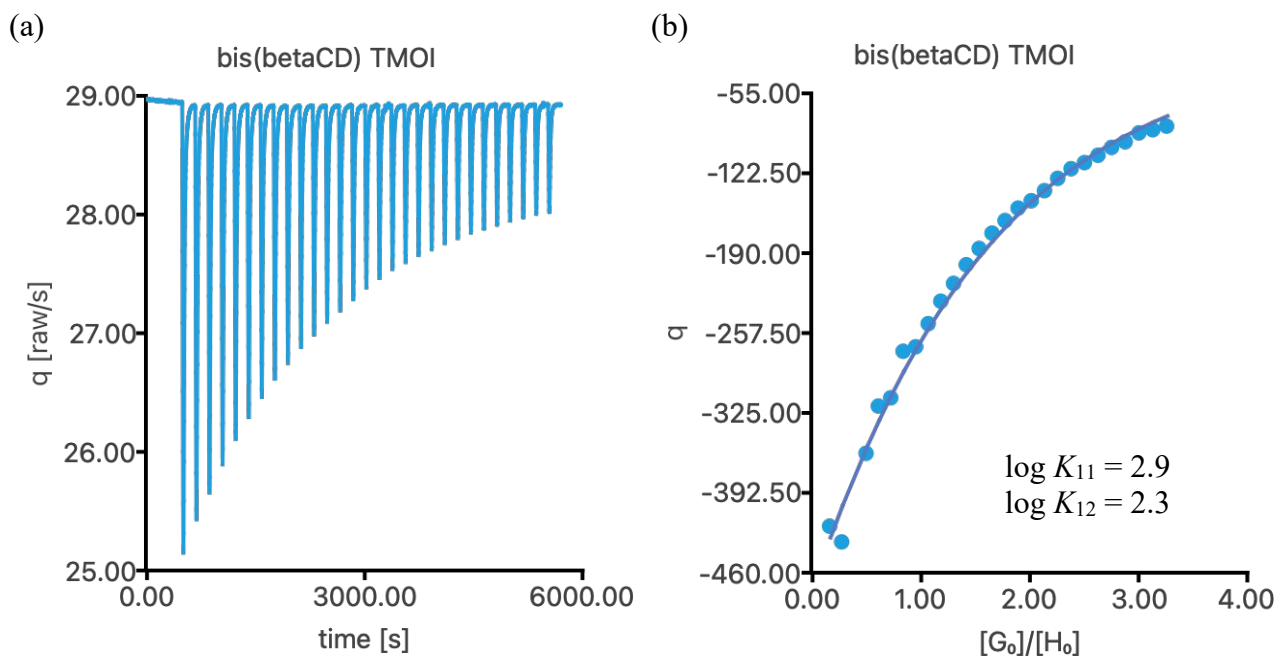


Figure S11: Thermogram (a) and binding isotherm (b) of the ITC titration of **b β CD** with **TMOI**. The data points in the isotherms are the experimental values and the line shows the fit of the data to the noncooperative 1:2 binding model.

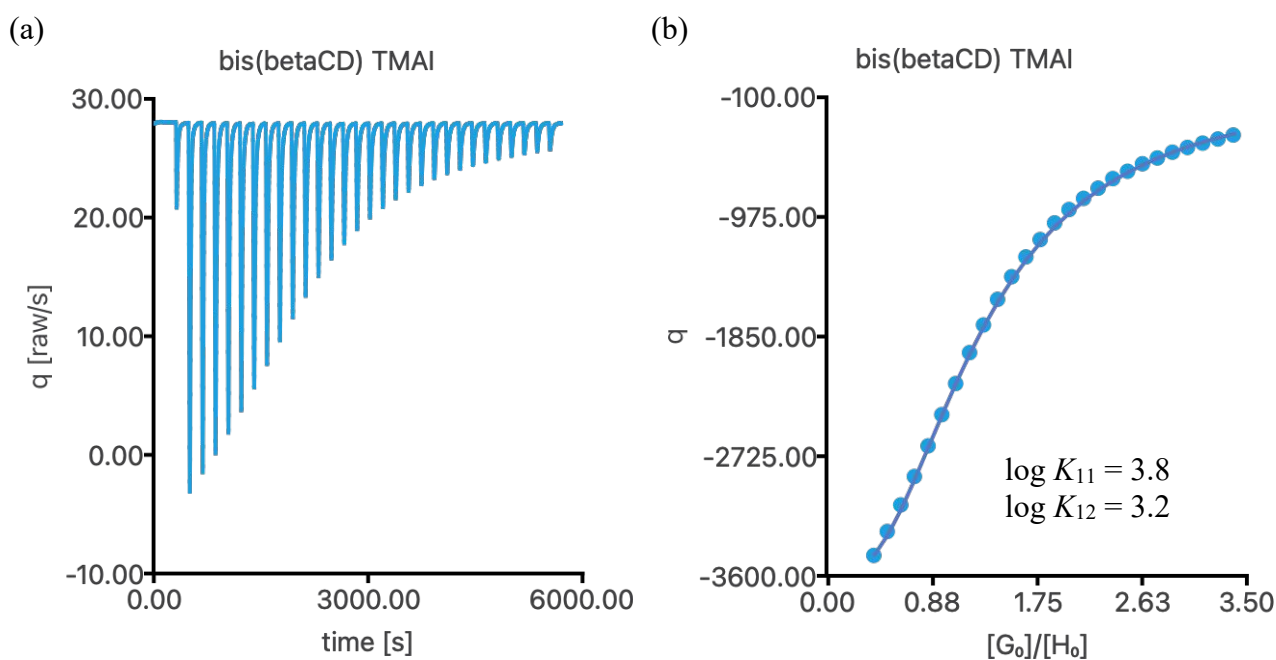


Figure S12: Thermogram (a) and binding isotherm (b) of the ITC titration of **b β CD** with **TMAI**. The data points in the isotherms are the experimental values and the line shows the fit of the data to the noncooperative 1:2 binding model.

Nanoparticle Synthesis and Characterisation

Analytical Methods

¹H NMR Spectroscopy. The ¹H NMR spectroscopic measurements were performed on a Bruker Avance™ III 400 spectrometer at 400 MHz and 25 °C. D₂O was used as purchased.

UV-vis Spectroscopy. The UV-vis measurements were performed by using a Varian Cary 100 spectrometer in semi-micro PMMA disposable cuvettes. All measurements were performed at 25 °C by using HPLC grade water as the solvent. The spectra were recorded between 350 and 800 nm. The AuNPs and the salts were weighed by using an analytical precision balance. Blank measurements were performed with water.

Transmission electron microscopy. A droplet of an aqueous AuNP solution was placed on a holey carbon grid (Plano S147-4) and dried under ambient conditions. A JEOL JEM-2100 LaB6 Transmission Electron Microscope (TEM) equipped with a Gatan Orius SC1000 CCD camera was used for bright-field imaging at 200 kV accelerating voltage. The images have a size of 1024×1024 pixels (acquisition time 0.5 s). The average diameters of the AuNPs were determined by processing the images with ImageJ followed by statistical analysis with MS Excel.

Determination of surface composition. For the assessment of the content of the cationic ligand on the surface of the mixed monolayer-protected nanoparticles, ¹H NMR spectra of solutions of the nanoparticles in D₂O were recorded. In the resulting spectrum, the integral of the multiplet between 3.4 and 3.7 ppm was set to 100 ($\int H^G = 100$). This signal was produced by 4 protons of **LG** (4-H, 6-H, 1×7-H, 13-H) and 1 proton of the cationic ligand (for both ligands 3-H). Then, characteristic signals of the cationic ligands were integrated (in the case of **LA**, the signal of the NMe₂ protons, and in the case of **LO** the signals of the NMe₂ and terminal CH₃ protons). The integral representing a single proton of the cationic ligand was calculated using the expression for **LO**:

$$\int H^C = \frac{\int \text{NMe}_2 + \int \text{CH}_3}{n_{\text{NMe}_2} + n_{\text{CH}_3}} = \frac{\int \text{NMe}_2 + \int \text{CH}_3}{9}$$

In the case of **LA**, $\int \text{CH}_3 = 0$ and $n_{\text{CH}_3} = 0$. The content of the cationic ligand is given by:

$$\%^C = \frac{\int H^C}{\frac{\int H^G - \int H^C}{n_G} + \int H^C} \times 100$$

This equation was rearranged to give:

$$\%^C = \frac{n_G \int H^C}{\int H^G + \int H^C (n_G - 1)} \times 100 = \frac{4 \int H^C}{100 + 3 \int H^C} \times 100$$

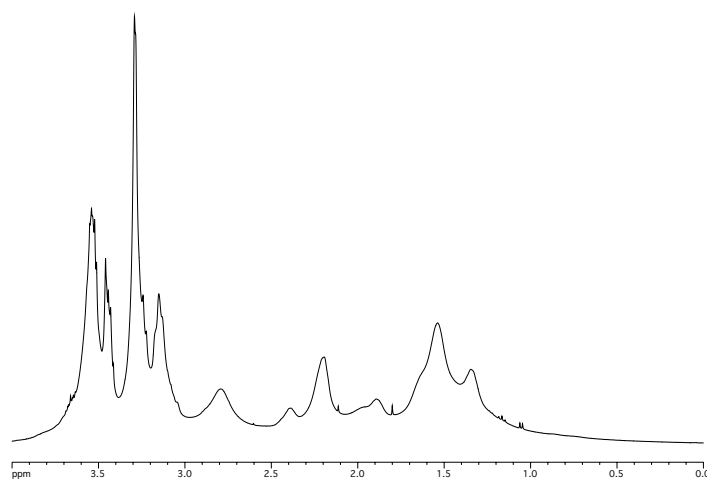
The error of the result was estimated to be $\pm 2.5\%$ (absolute), especially for nanoparticles with a lower content of the cationic ligand whose signals were small and overlapped with signals of **LG** in the ^1H NMR spectrum.

Syntheses

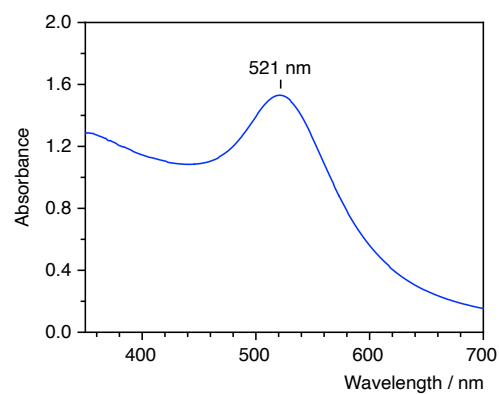
AuNP stock solution.⁸ For the seed solution, tetrachloroauric acid (8.50 mg, 25.0 μmol) and trisodium citrate (7.40 mg, 28.7 μmol) were dissolved in water (100 mL) and mixed with a cold solution of sodium borohydride (100 mM, 3 mL) in water. The red solution was stirred for 2 h at 25 $^\circ\text{C}$. For the growth step, a solution of cetyltrimethylammonium bromide (270 mg, 740 μmol) in water (9 mL) was mixed with ascorbic acid (100 mM, 0.5 mL) and the previously prepared seed solution (10 mL) was added. Tetrachloroauric acid (8.50 mg, 25.0 μmol) was then dissolved in water (1 mL) and added to the reaction mixture while stirring vigorously. The resulting red solution was stirred for 1 h at 25 $^\circ\text{C}$. This solution was directly used as the stock solution for further functionalisation.

AuNP^{LG}. A solution of **LG** (750 μL , 0.1 M in water) was added to the **AuNP** stock solution (20.5 mL), and the reaction mixture was stirred for 1 h at 25 $^\circ\text{C}$. The mixture was then washed with chloroform (3 \times 50 mL) using centrifugation (4400 rpm, 20 $^\circ\text{C}$) for phase separation and the resulting solution was stirred in an open flask overnight under the fume hood to ensure that residual chloroform had completely evaporated (the membranes used in the next step are not stable in the presence of chloroform). Next, the nanoparticle solution was transferred into centrifugal concentrators (Vivaspin 500 centrifugal concentrators MWCO 5 kDa) and filtered by centrifugation (3000 rpm, 20 $^\circ\text{C}$). The particles were resuspended in water and membrane filtration was repeated three times. The resulting AuNPs were collected, and the solvent was removed under reduced pressure. Yield: 7.4 mg.

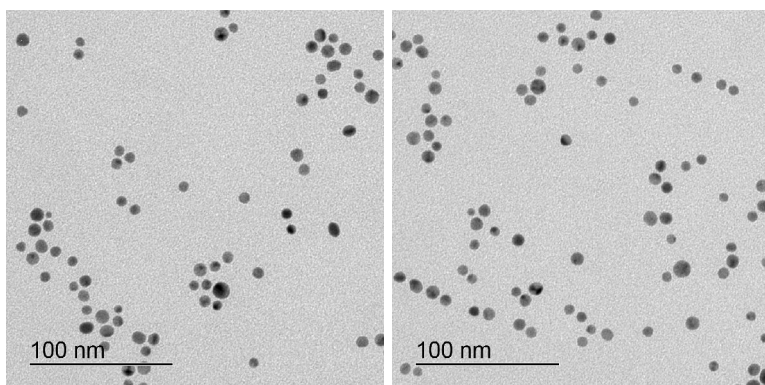
(a)



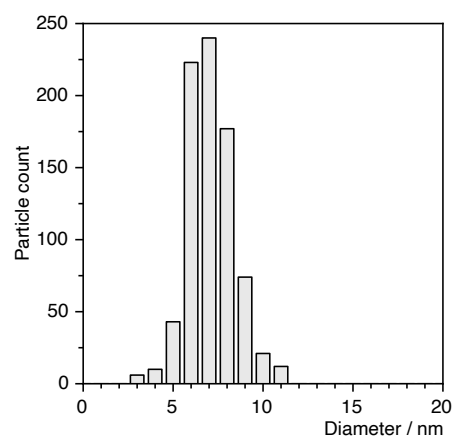
(b)



(c)



(d)

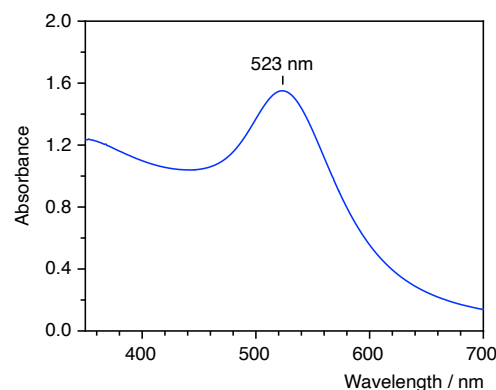
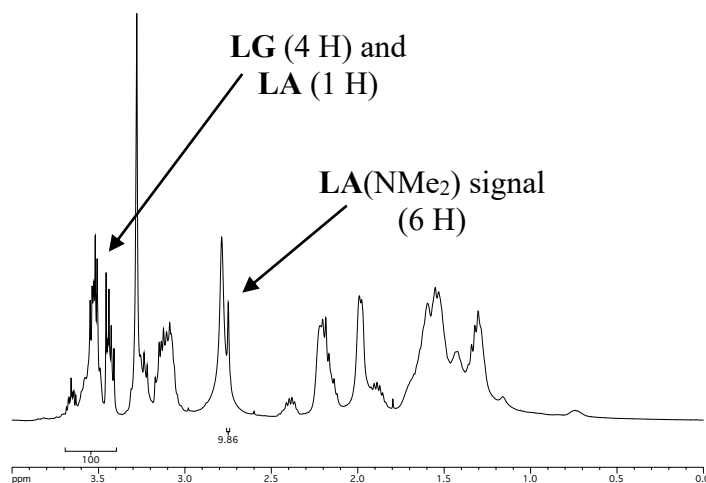


average diameter: 7.6 ± 1.3 nm

Figure S13: ^1H NMR spectrum in D_2O (a) and UV-vis spectrum (b) of AuNP^{LG} in water, and TEM image (c) together with the histogram illustrating the size distribution of the nanoparticles derived from the TEM image (d).

AuNP^{6LA}. A mixture of **LG** (500 μ L, 0.1 M in water) and **LA** (250 μ L, 0.1 M in methanol) were added to the **AuNP** stock solution (20.5 mL), and the reaction mixture was stirred for 1 h at 25 $^{\circ}$ C. The nanoparticles were purified as described for **AuNP^{LG}**. Yield: 9.8 mg.

(a) (b)

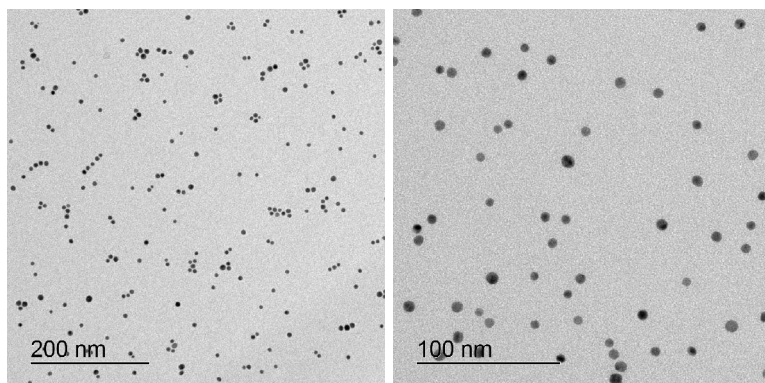


Relative content of the cationic ligand:

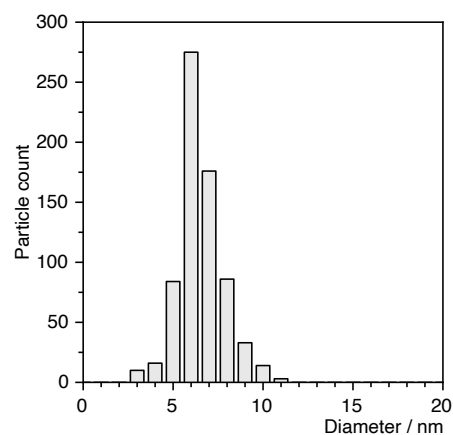
$$\int H^c = \frac{9.86}{6}$$

$$\%^c = \frac{4 \int H^c}{100 + 3 \int H^c} \times 100 = 6\%$$

(c)



(d)

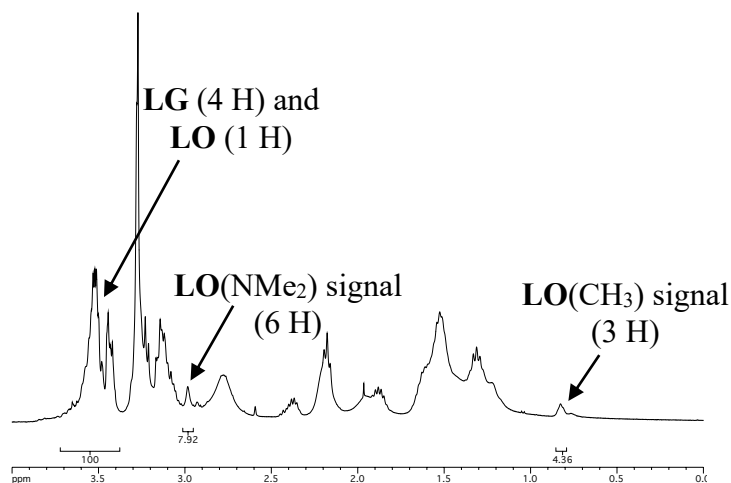


average diameter: 7.0 ± 1.2 nm

Figure S14: ^1H NMR spectrum of **AuNP^{6LA}** in D_2O (a) and UV-vis spectrum (b) of **AuNP^{6LA}** in water, and TEM image (c) together with the histogram illustrating the size distribution of the nanoparticles derived from the TEM image (d).

AuNP^{5LO}. A mixture of **LG** (2250 μ L, 0.025 M in water) and **LO** (750 μ L, 0.025 M in methanol) were added to the **AuNP** stock solution (20.5 mL), and the reaction mixture was stirred for 1 h at 25 $^{\circ}$ C. The nanoparticles were purified as described for **AuNP^{LG}**. Yield: 7.7 mg.

(a)

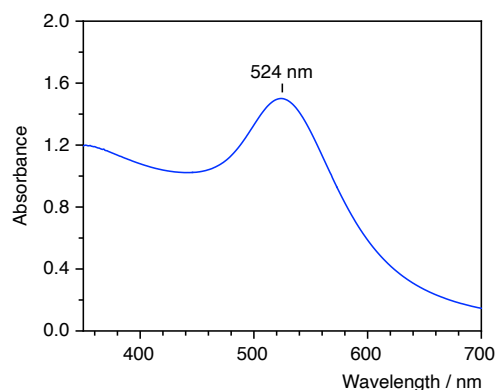


Relative content of the cationic ligand:

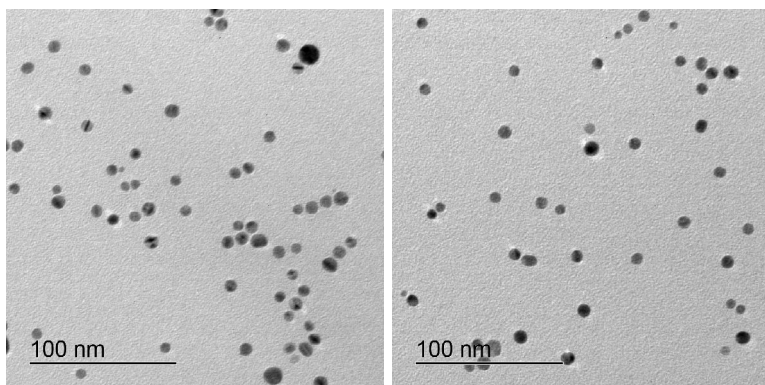
$$\int H^c = \frac{7.92 + 4.36}{9}$$

$$\%^c = \frac{4 \int H^c}{100 + 3 \int H^c} \times 100 = 5\%$$

(b)



(c)



average diameter: 8.0 ± 1.2 nm

(d)

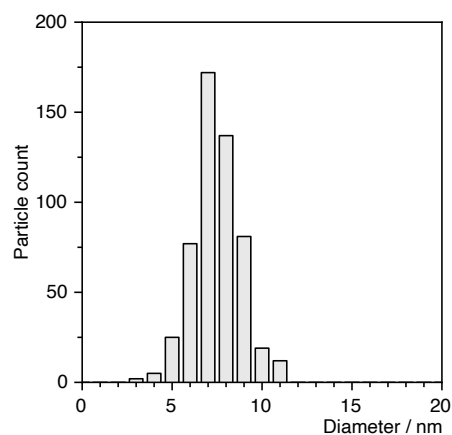
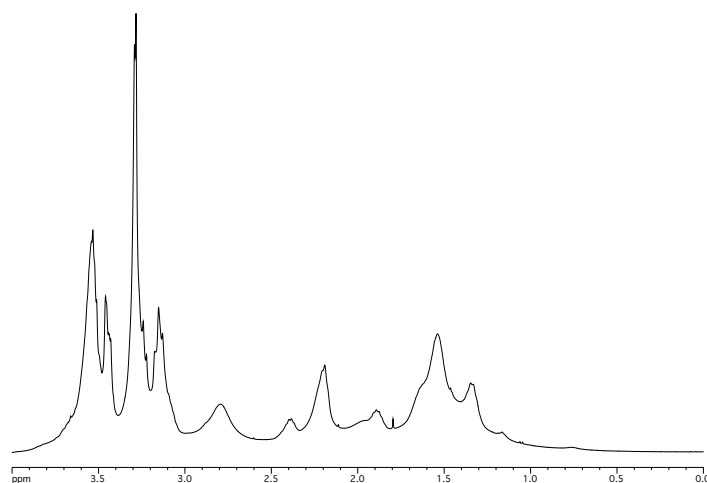


Figure S15: ^1H NMR spectrum of **AuNP^{5LO}** in D_2O (a) and UV-vis spectrum (b) of **AuNP^{5LO}** in water, and TEM image (c) together with the histogram illustrating the size distribution of the nanoparticles derived from the TEM image (d).

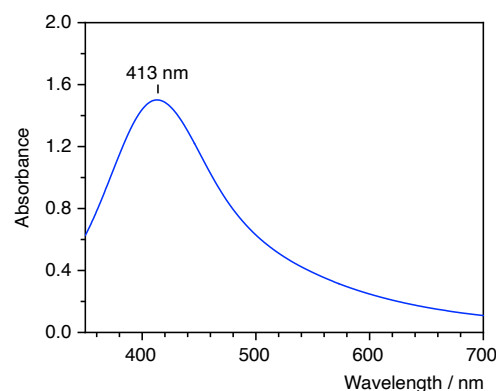
AgNP stock solution.⁹ Nitrogen was bubbled through an aqueous solution of sodium borohydride (2.04 M, 17.0 mL) under ice bath cooling for 15 min. This solution was added to a solution of silver nitrate (1.04 mM, 4.00 mL) in water under vigorous stirring. The mixture was stirred for 2 h at 25 °C and immediately used for the functionalisation.

AgNP^{LG}. A solution of **LG** (750 µL, 0.1 M in water) was added to the **AgNP** stock solution (21 mL), and the reaction mixture was stirred for 2 h at 25 °C. The resulting nanoparticles were isolated and purified by membrane centrifugation as described for **AuNP**. The particles thus obtained were collected and the solution freeze-dried. Yield: 2.1 mg.

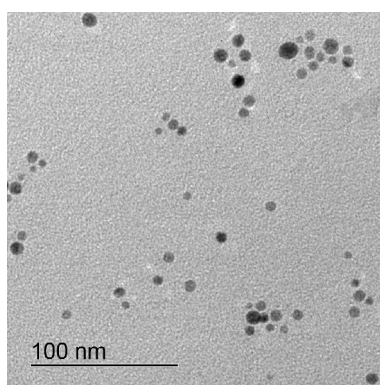
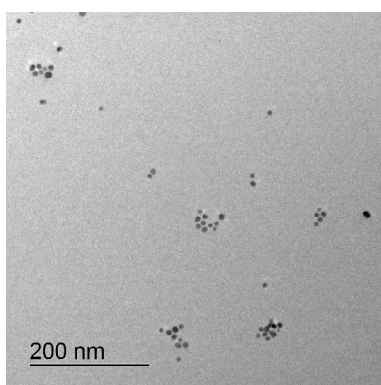
(a)



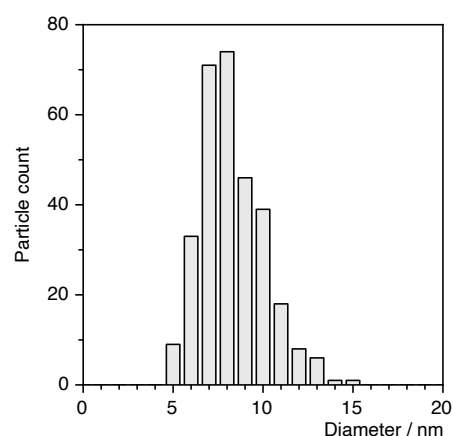
(b)



(c)



(d)

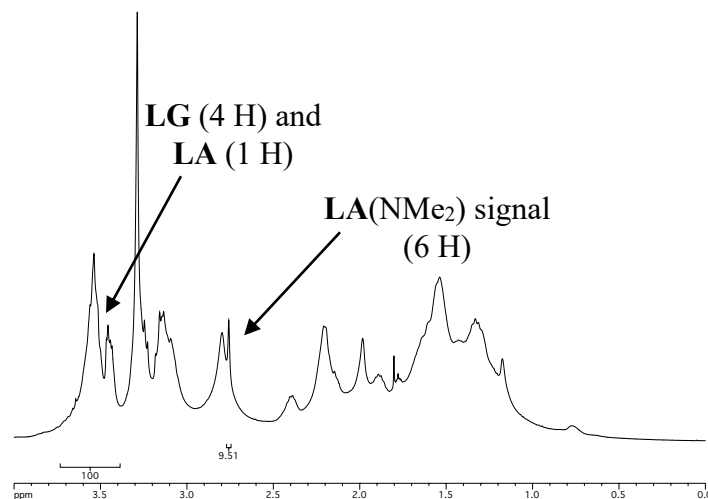


average diameter: 8.8 ± 1.8 nm

Figure S16: ^1H NMR spectrum in D_2O (a) and UV-vis spectrum (b) of **AgNP^{LG}** in water, and TEM image (c) together with the histogram illustrating the size distribution of the nanoparticles derived from the TEM image (d).

AgNP^{6LA}. A mixture of **LG** (500 μ L, 0.1 M in water) and **LA** (250 μ L, 0.1 M in methanol) were added to the **AgNP** stock solution (21 mL), and the reaction mixture was stirred for 2 h at 25 $^{\circ}$ C. The nanoparticles were purified as described for **AgNP^{LG}**. Yield: 1.4 mg.

(a)

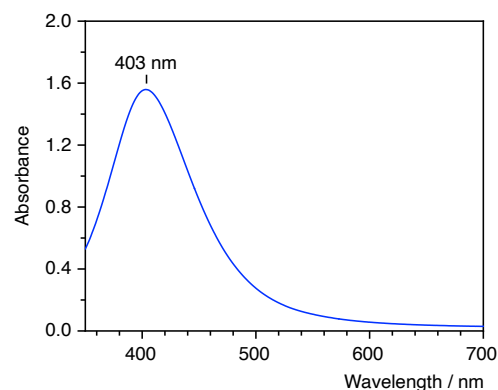


Relative content of the cationic ligand:

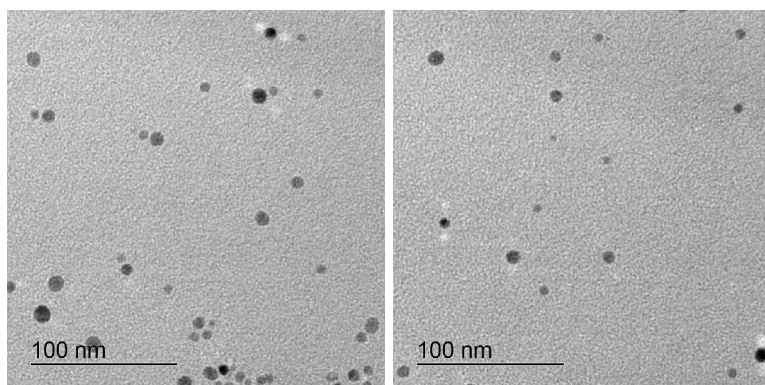
$$\int H^c = \frac{9.51}{6}$$

$$\%^c = \frac{4 \int H^c}{100 + 3 \int H^c} \times 100 = 6\%$$

(b)



(c)



average diameter: 9.1 ± 2.3 nm

(d)

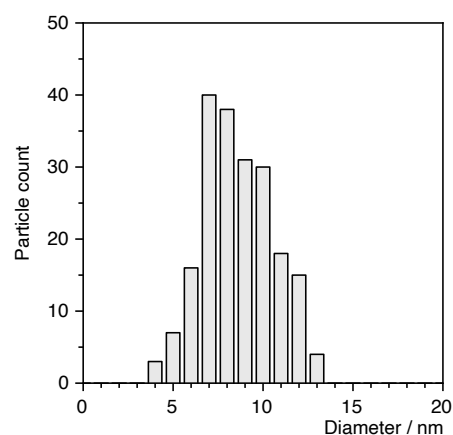
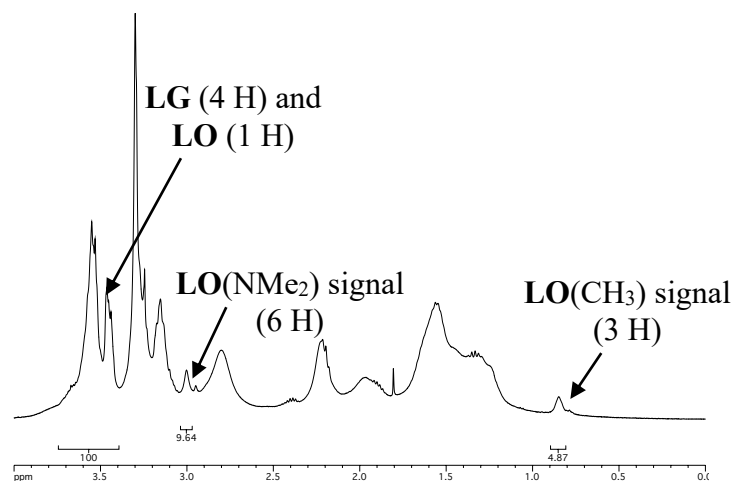


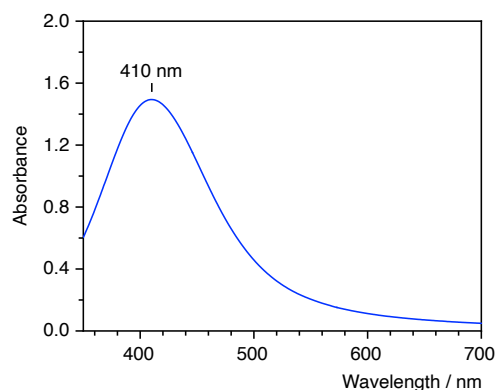
Figure S17: ^1H NMR spectrum of **AgNP^{6LA}** in D_2O (a) and UV-vis spectrum (b) of **AgNP^{6LA}** in water, and TEM image (c) together with the histogram illustrating the size distribution of the nanoparticles derived from the TEM image (d).

AgNP^{6LO}. A mixture of **LG** (2000 μ L, 0.025 M in water) and **LO** (1000 μ L, 0.025 M in methanol) were added to the **AgNP** stock solution (21 mL), and the reaction mixture was stirred for 2 h at 25 $^{\circ}$ C. The nanoparticles were purified as described for **AgNP^{LG}**. Yield: 3.0 mg.

(a)



(b)

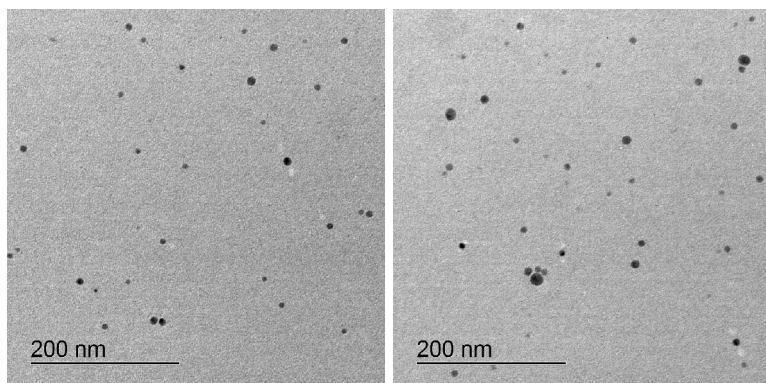


Relative content of the cationic ligand:

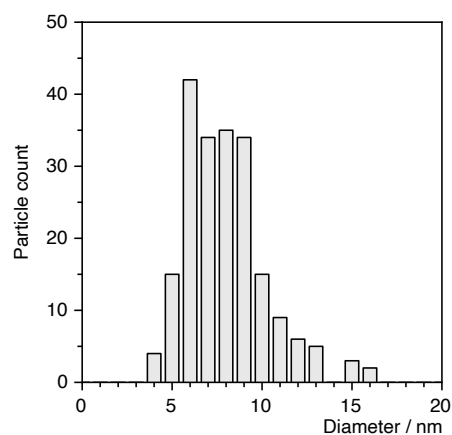
$$\int H^c = \frac{9.64 + 4.87}{9}$$

$$\%c = \frac{4 \int H^c}{100 + 3 \int H^c} \times 100 = 6\%$$

(c)



(d)



average diameter: 8.6 ± 2.3 nm

Figure S18: ^1H NMR spectrum of **AgNP^{6LO}** in D_2O (a) and UV-vis spectrum (b) of **AgNP^{6LO}** in water, and TEM image (c) together with the histogram illustrating the size distribution of the nanoparticles derived from the TEM image (d).

Binding Studies

Visual Binding Study. All solutions used in these experiments were prepared by using HPLC grade water. Six vials, each containing 200 μL of the sample solutions, were prepared and placed on a piece of paper to create a white background. The two vials on the left contained solutions of silver nanoparticles, the two samples on the right contained solutions of gold nanoparticles, and the two middle vials contained mixtures. The gold and silver nanoparticle solutions were prepared by dissolving the respective nanoparticles in water and diluting the solutions until they were brightly coloured. The mixture was prepared from the undiluted silver and the gold nanoparticle stock solutions by combining and diluting them to a bright orange colour. In general, more of the silver nanoparticle solution was used. An aqueous bis(cyclodextrin) solution (10 mM) was added to the second, fourth and sixth vial (from the left). To all other vials, the same volume of water was added. The first addition was 10.6 μL to obtain a bis(cyclodextrin) concentration of 500 μM . Photographs were taken after 15 min and when no further changes in the bis(cyclodextrin)-containing solutions could be observed. More of the bis(cyclodextrin) solution (11.6 μL) was then added to increase the concentration to 1000 μM . Photographs were taken after 15 min and at equilibrium. If necessary, the bis(cyclodextrin) concentration was further increased to 1500 μM and 2000 μM by adding 13.1 μL and further 14.7 μL of the bis(cyclodextrin) stock solution, respectively, and the colour changes followed. The photographs of the various experiments are shown in Figures S24-S31.

UV-vis Spectroscopic Binding Study. Measurements were performed at 22 $^{\circ}\text{C}$ by using semi-micro PMMA disposable cuvettes with a 1 cm path length and HPLC grade water as solvent and in the reference cell. The solutions containing gold or silver nanoparticles were prepared by dissolving these nanoparticles in water and diluting the resulting solutions until the absorbance of the respective SPR bands was 1.5. Mixtures were prepared from the thus obtained silver nanoparticle solution by adding the undiluted gold nanoparticle stock solution until the absorbance at the maximum wavelength of the gold SPR band was approximately 1.25. Note that the resulting absorbance of this solution in the wavelength region of the silver nanoparticle SPR band was higher than 1.5 because the gold nanoparticles also absorb in this region.

Each series of measurements was carried out in one cuvette. In the first measurement, the nanoparticle solution (1 mL) was added to the cuvette and the UV-vis spectrum was recorded between 350 nm (or 400 nm if the solution contained only gold nanoparticles) and 700 nm. For subsequent measurements, a defined volume of bis(cyclodextrin) solution (10 mM) was added, the cuvette shaken, the UV-vis spectrum recorded 10 minutes after the addition, and then the next addition was made. The exact amounts of bis(cyclodextrin) solutions and the order of addition are summarised in Table S3.

Table S3: Added volumes of bis(cyclodextrin) solution of salt solutions and sequence of addition to the nanoparticle solution in water/methanol, 1:2 (v/v) and concentrations resulting after each addition

Entry	V (bis(cyclodextrin) solution) / μL	V total / μL	c (bis(cyclodextrin)) / μM
1	0	1000.0	0
2	10.1	1010.1	100
3	10.3	1020.4	200
4	10.5	1030.9	300
5	10.8	1041.7	400
6	10.9	1052.6	500
7	14.1	1066.7	625
8	14.4	1081.1	750
9	14.8	1095.9	875
10	15.2	1111.1	1000
11	31.8	1142.9	1250
12	33.6	1176.5	1500
13	35.6	1212.1	1750
14	37.9	1250.0	2000
15	40.3	1290.3	2250
16	43.0	1333.3	2500

The UV-vis spectra of the binding studies involving single nanoparticles are shown in Figures S19–S22. Spectra of nanoparticle mixtures are shown in Figures S24–S31 together with the results of the visual binding studies. Spectra of mixtures were recorded by using the procedure described above, but by performing the titration only until the bis(cyclodextrin) concentration was 500 or 1000 μM .

Transmission Electron Microscopy. For the images of the gold and silver nanoparticles, the stock solutions of the respective nanoparticles were diluted with water and the resulting solutions were

immediately used for the measurements. Images of mixtures were taken from 1:1 (v/v) mixtures of the solutions of the individual nanoparticles. To assess the effect of bis(cyclodextrin) addition, an aqueous solution of a bis(cyclodextrin) (10 mM, 22.2 μ L) was added to a nanoparticle solution (200 μ L). The solution was shaken, and the TEM image recorded after 3 d. For each measurement, a droplet of the solution was placed on a holey carbon grid (Plano S147-4) and dried under ambient conditions. TEM images of the individual nanoparticles are shown in Figures S13-S18, and TEM images of the mixtures in Figures S24-S31.

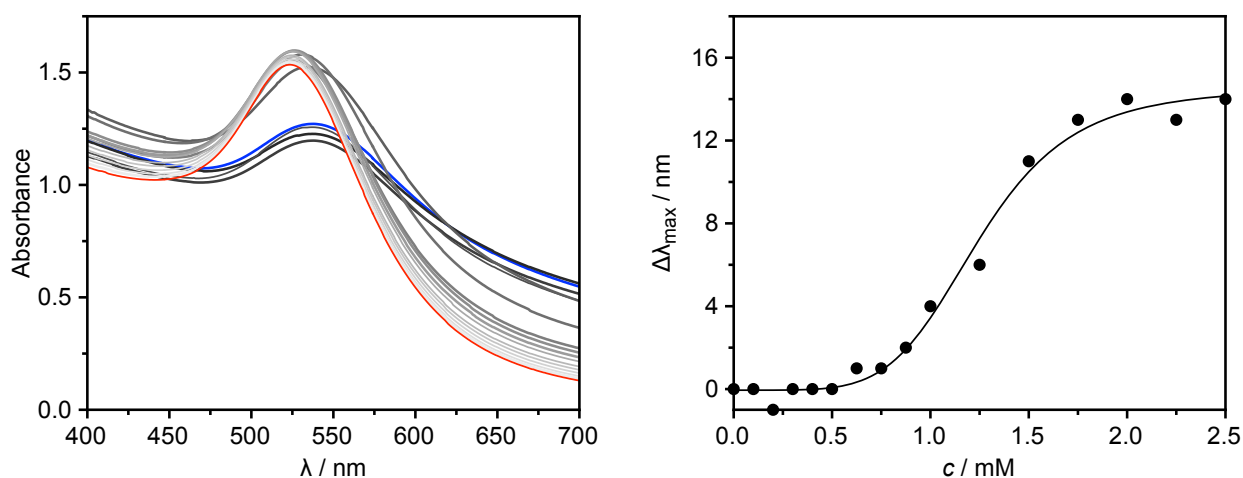


Figure S19: UV-vis spectroscopic binding study and the Hill plot derived from these spectra for the combination **AuNP^{6LA}** and **baCD** in water (the Hill plot is also shown in Fig. 2 of the main article).

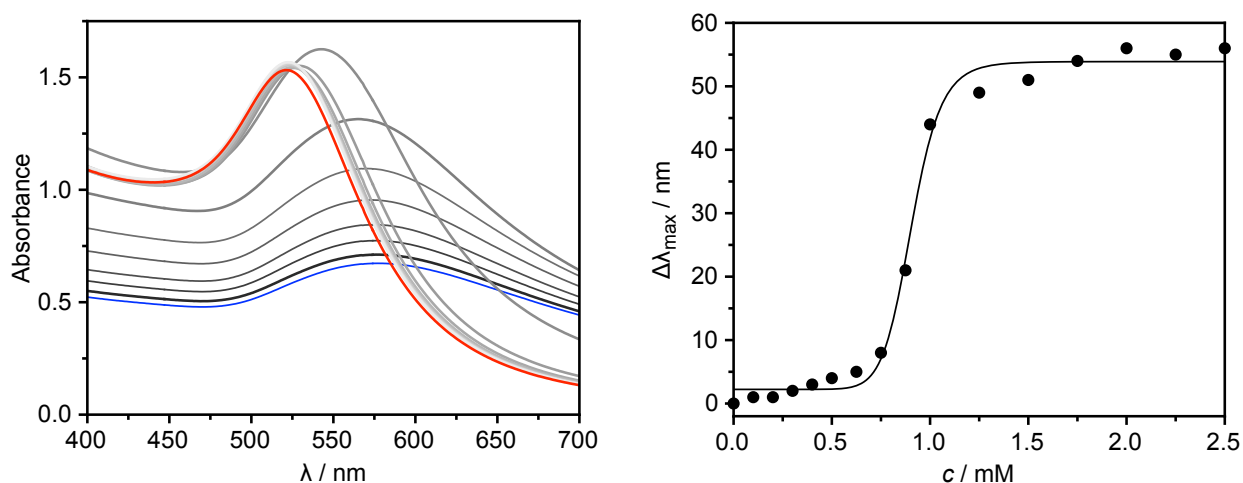


Figure S20: UV-vis spectroscopic binding study and the Hill plot derived from these spectra for the combination **AuNP^{6LA}** and **b β CD** in water (the spectra and the corresponding Hill plot is also shown in Fig. 1 and Fig. 2 of the main article).

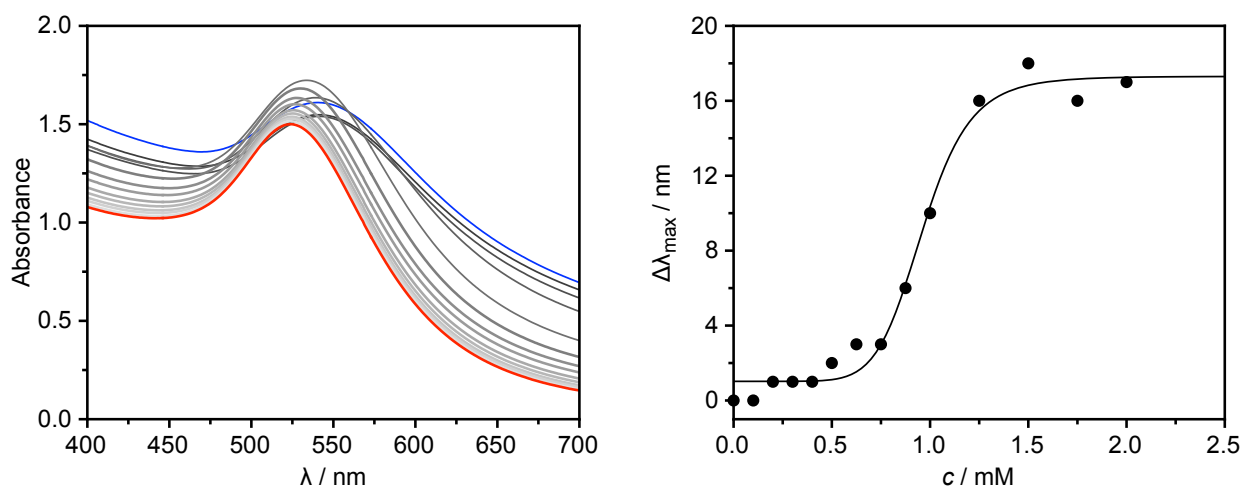


Figure S21: UV-vis spectroscopic binding study and the Hill plot derived from these spectra for the combination **AuNP^{5LO}** and **βαCD** in water (the Hill plot is also shown in Fig. 2 of the main article).

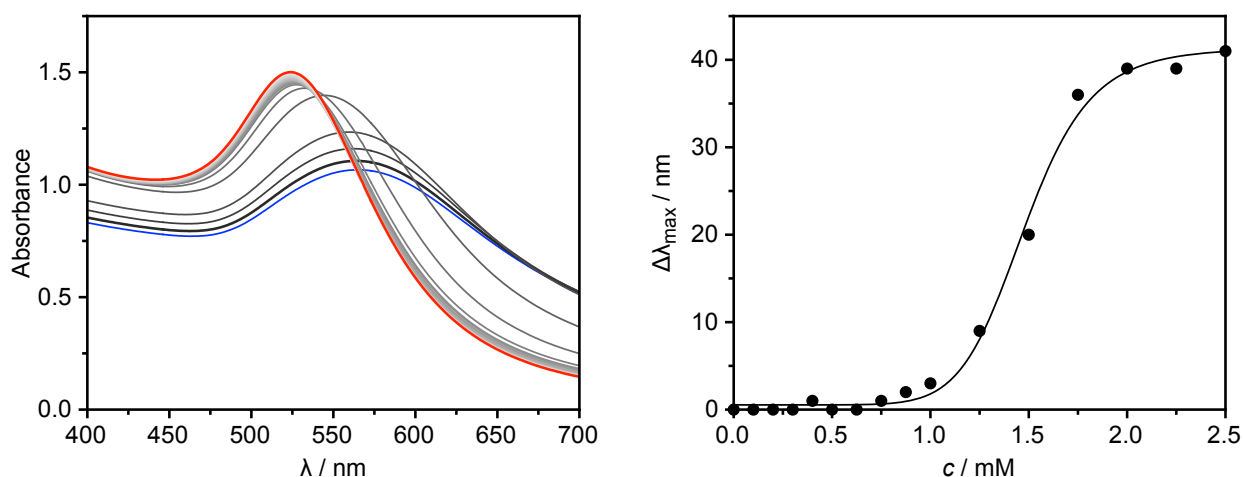


Figure S22: UV-vis spectroscopic binding study and the Hill plot derived from these spectra for the combination **AuNP^{5LO}** and **bβCD** in water (the Hill plot is also shown in Fig. 2 of the main article).

In addition, titrations were performed in the presence of an excess of α CD or β CD (1 mM or 5 mM). To this end, the required amount of the corresponding cyclodextrin was weighed into a cuvette, the nanoparticle solution was added, and the titration was performed as described above after complete dissolution. The binding plot thus obtained are compared in Figure S23 with those obtained for the same nanoparticle bis(cyclodextrin) combination in the absence of the cyclodextrins.

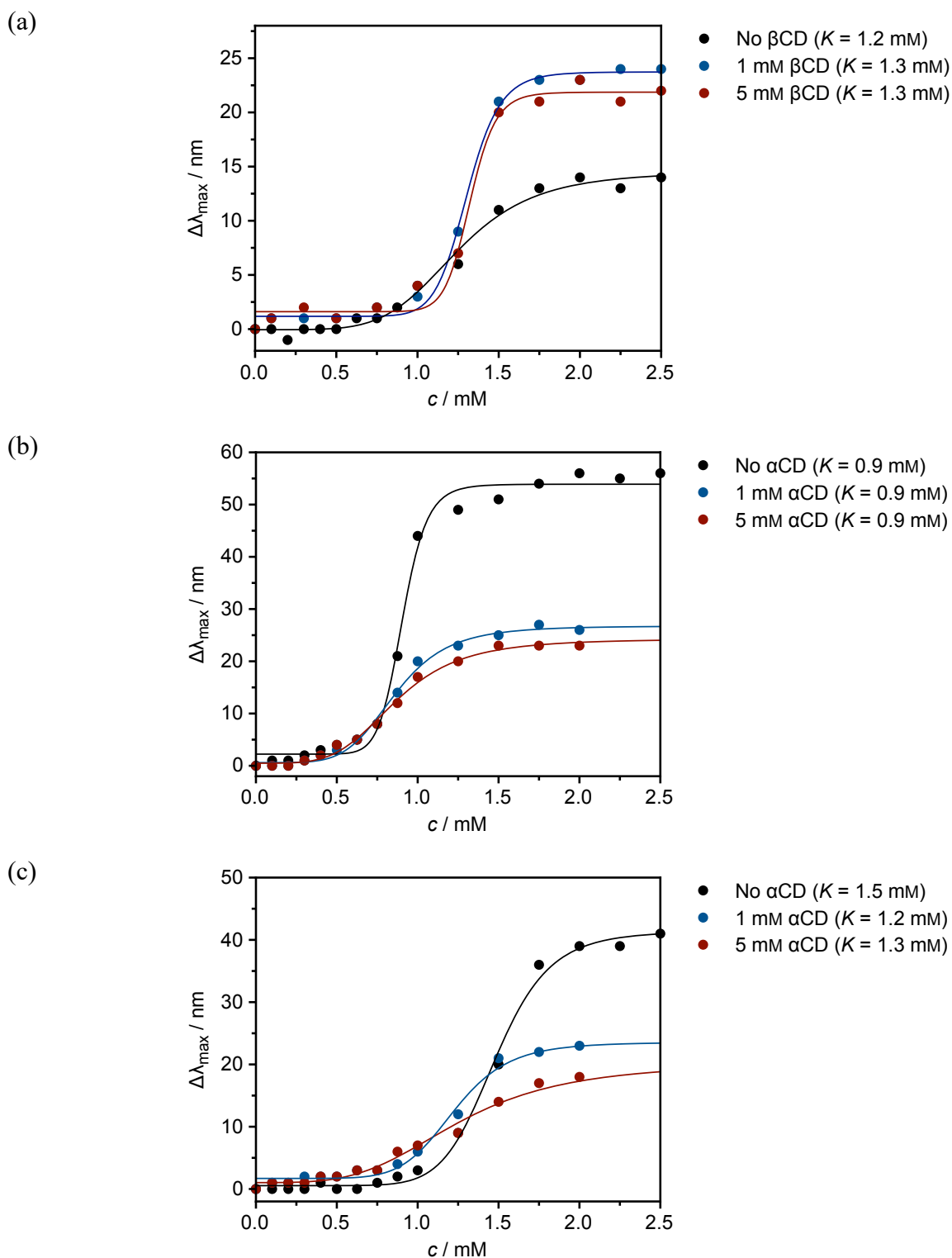
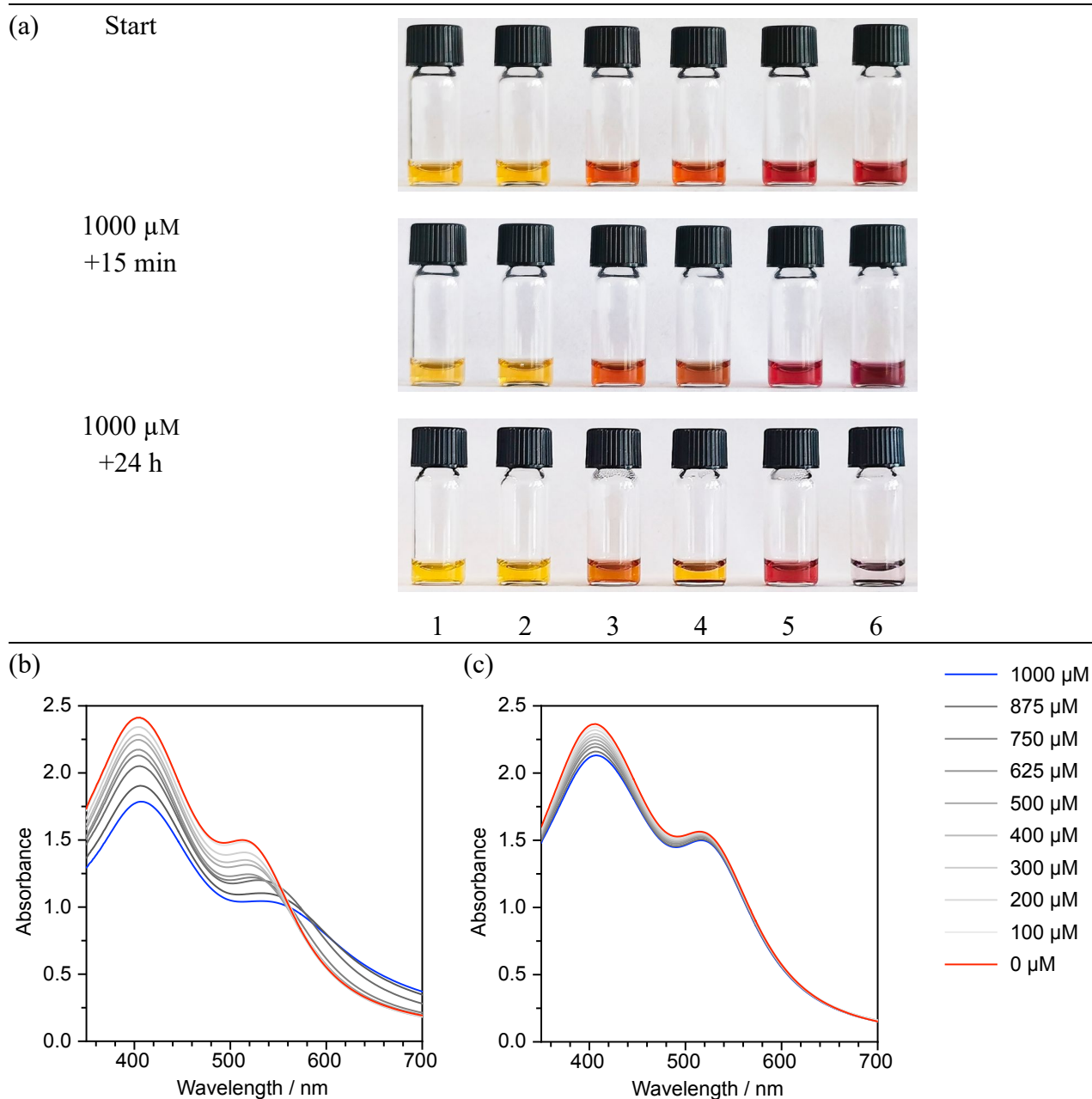


Figure S23: Hill plots derived from UV-vis spectroscopic binding studies showing the effect of β CD on the **α CD**-mediated aggregation of **AuNP^{6LA}** (a), α CD on the **β CD**-mediated aggregation of **AuNP^{6LA}** (b), and α CD on the **β CD**-mediated aggregation of **AuNP^{5L0}** (c).

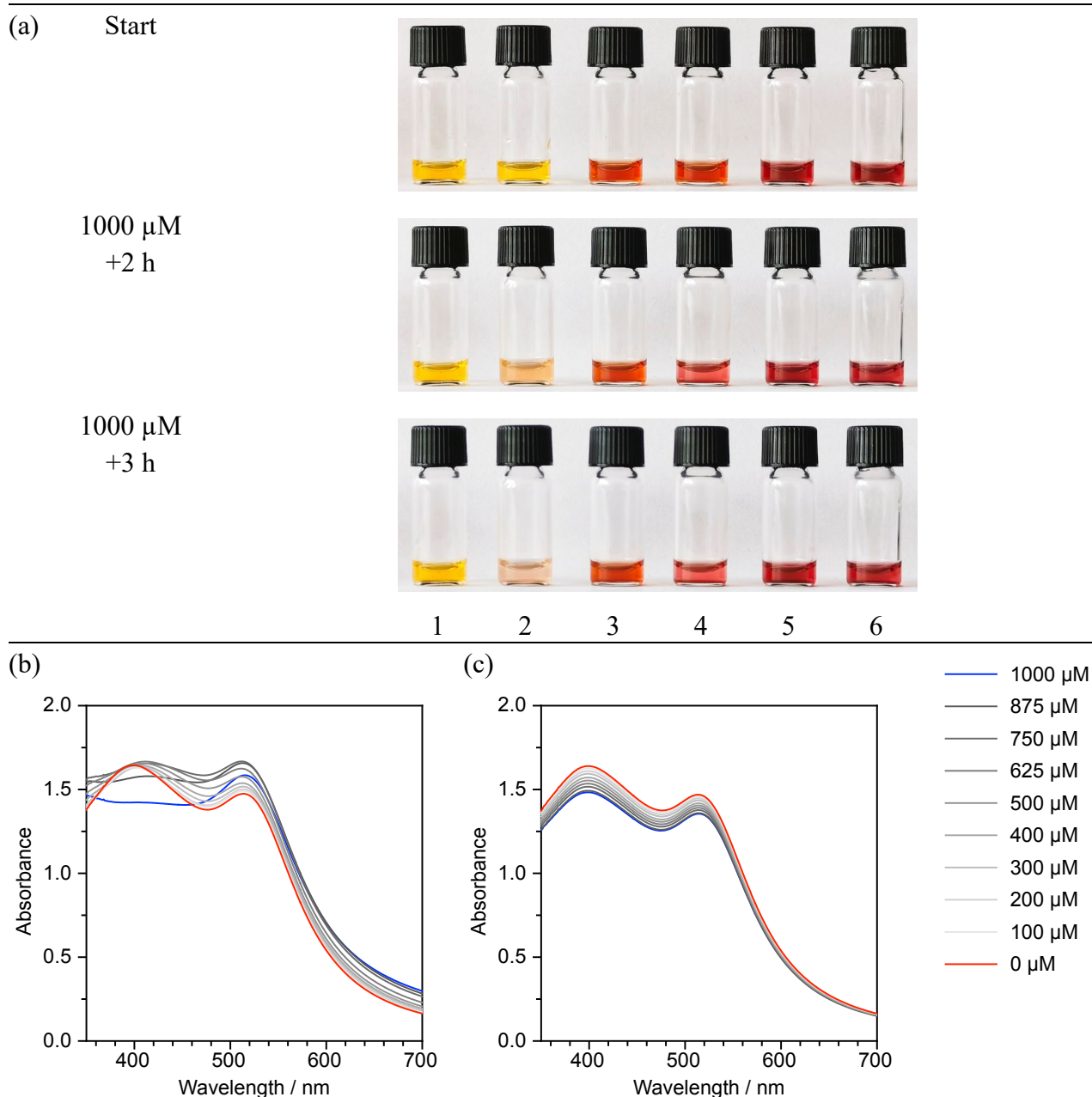
The graphs in Figure S23 show that the presence of the cyclodextrins affects the extent to which the SPR of the gold nanoparticle is shifted during aggregation, while the concentration of

bis(cyclodextrin) required to mediate aggregation is virtually unaffected. The first effect is difficult to interpret due to the lack of structural information about the host-guest interactions at the nanoparticle surface. Nevertheless, it is interesting to note that the presence of β CD causes an increase in the shift of the SPR band with respect to the shift in the absence of cyclodextrin, while α CD had the opposite effect. The lack of effect of the cyclodextrins on the K values is probably due to the multivalency associated with nanoparticle aggregation, which causes the strength of the interactions to be substantially stronger than that of a single host-guest interaction, even when only a few surface-bound groups are involved.



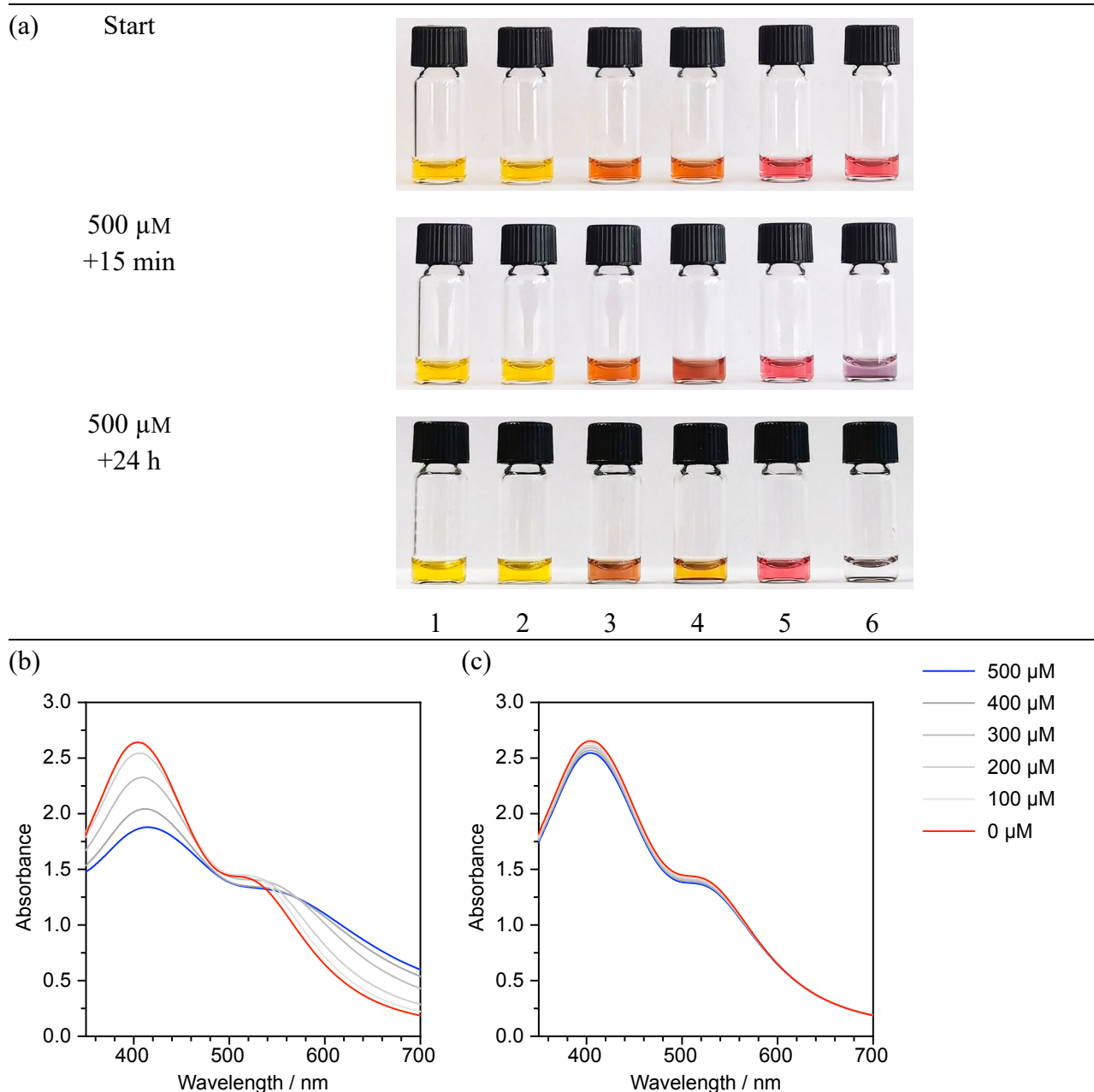
Only **AuNP^{6LA}** precipitated upon addition of the bis(cyclodextrin) while the unfunctionalised **AgNP^G** was not affected. In the UV-vis spectroscopic study, only the SPR band of **AuNP^{6LA}** moved to longer wavelengths. In contrast, the monotopic cyclodextrin did not produce an effect.

Figure S24: Visual (a) and UV-vis spectroscopic binding study (b) for the combination **AgNP^G**, **AuNP^{6LA}**, and **bβCD**. In (a), vials 1 and 2 contain solutions of **AgNP^G**, vials 5 and 6 solutions of **AuNP^{6LA}**, and vials 3 and 4 mixtures of these nanoparticles in water. The aqueous **bβCD** solution was added to vials 2, 4, and 6, while an equivalent amount of water was added to vials 1, 3, and 5. The UV-vis spectra in (c) show the results for the UV-vis spectroscopic binding study when **βCD** was used instead of the corresponding bis(cyclodextrin).



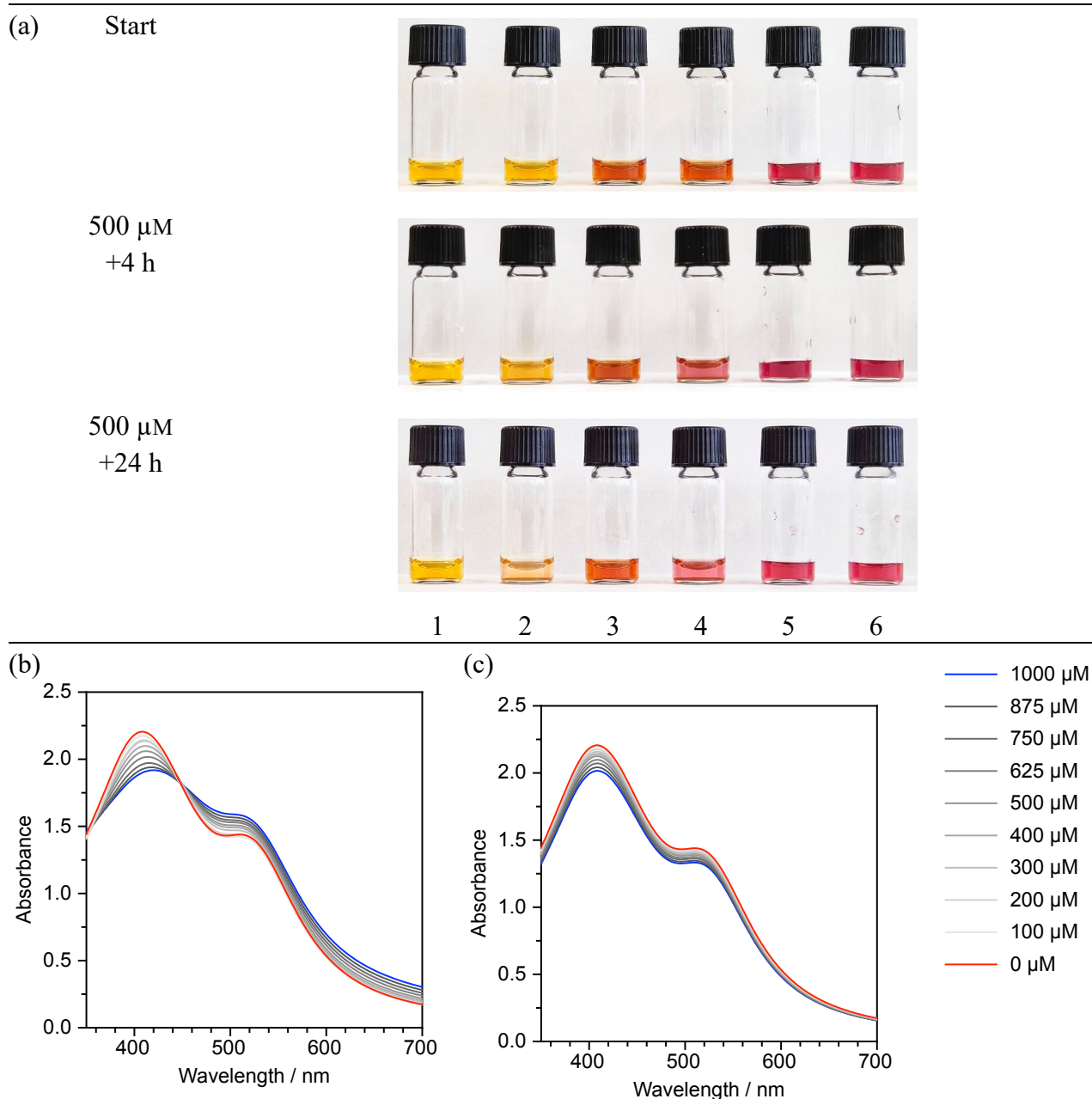
Only the **AgNP^{6LA}** solution changed colour upon the addition of the bis(cyclodextrin) while the solution of **AuNP^G** was not affected. In the UV-vis spectroscopic study, the SPR band of **AgNP^{6LA}** gradually disappeared. In contrast, the monotopic cyclodextrin did not produce an effect.

Figure S25: Visual (a) and UV-vis spectroscopic binding study (b) for the combination **AgNP^{6LA}**, **AuNP^G**, and **bβCD**. In (a), vials 1 and 2 contain solutions of **AgNP^{6LA}**, vials 5 and 6 solutions of **AuNP^G**, and vials 3 and 4 mixtures of these nanoparticles in water. The aqueous **bβCD** solution was added to vials 2, 4, and 6, while an equivalent amount of water was added to vials 1, 3, and 5. The UV-vis spectra in (c) show the results for the UV-vis spectroscopic binding study when **βCD** was used instead of the corresponding bis(cyclodextrin).



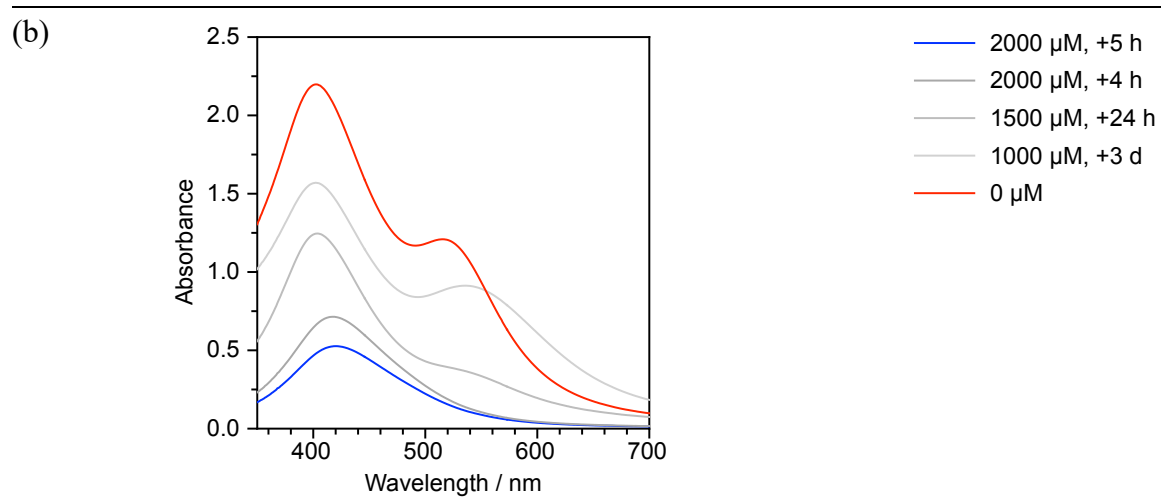
Only the $\text{AuNP}^{5\text{LO}}$ solution changed colour upon the addition of the bis(cyclodextrin) while the AgNP^{G} solution was not affected. In the UV-vis spectroscopic study, only the SPR band of $\text{AuNP}^{5\text{LO}}$ moved to longer wavelengths. In contrast, the monotopic cyclodextrin did not produce an effect.

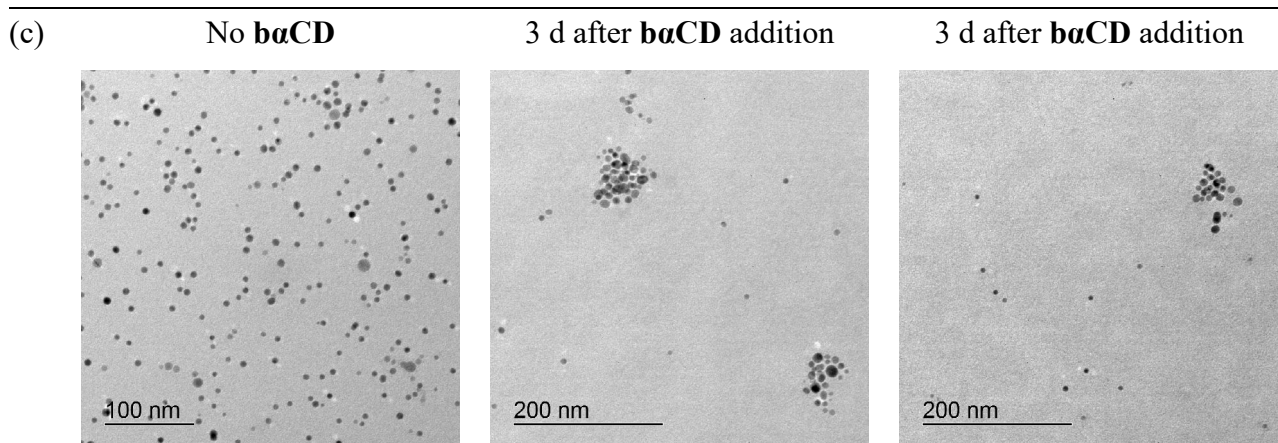
Figure S26: Visual (a) and UV-vis spectroscopic binding study (b) for the combination AgNP^{G} , $\text{AuNP}^{5\text{LO}}$, and $\beta\alpha\text{CD}$. In (a), vials 1 and 2 contain solutions of AgNP^{G} , vials 5 and 6 solutions of $\text{AuNP}^{5\text{LO}}$, and vials 3 and 4 mixtures of these nanoparticles in water. The aqueous $\beta\alpha\text{CD}$ solution was added to vials 2, 4, and 6, while an equivalent amount of water was added to vials 1, 3, and 5. The UV-vis spectra in (c) show the results for the UV-vis spectroscopic binding study when αCD was used instead of the corresponding bis(cyclodextrin).



Only the $\text{AgNP}^{6\text{LO}}$ solution changed colour upon the addition of the bis(cyclodextrin) while the AuNP^{G} solution was not affected. In the UV-vis spectroscopic study, only the SPR band of $\text{AgNP}^{6\text{LO}}$ moved to longer wavelengths. In contrast, the monotopic cyclodextrin did not produce an effect.

Figure S27: Visual (a) and UV-vis spectroscopic binding study (b) for the combination $\text{AgNP}^{6\text{LO}}$, AuNP^{G} , and baCD . In (a), vials 1 and 2 contain solutions of $\text{AgNP}^{6\text{LO}}$, vials 5 and 6 solutions of AuNP^{G} , and vials 3 and 4 mixtures of these nanoparticles in water. The aqueous baCD solution was added to vials 2, 4, and 6, while an equivalent amount of water was added to vials 1, 3, and 5. The UV-vis spectra in (c) show the results for the UV-vis spectroscopic binding study when αCD was used instead of the corresponding bis(cyclodextrin).





Average diameter of the non-aggregated nanoparticles: 10.0 ± 3.4 nm

The solution containing **AuNP^{5LO}** turned blue and eventually became colourless in the presence of **ba**CD while the colour of the **AgNP^{6LA}** solution remained unchanged. Precipitation of the latter nanoparticles only occurred at a higher concentration of the bis(cyclodextrin). In the UV-vis spectroscopic binding study, the SPR band of **AuNP^{5LO}** decreased in intensity until no clear band was visible anymore. The SPR band of **AgNP^{6LA}** persisted longer. The TEM images in (c) illustrate that only part of the nanoparticles initially aggregated in the presence of the bis(cyclodextrin).

Figure S28: Visual (a) and UV-vis spectroscopic binding study (b) for the combination **AgNP^{6LA}**, **AuNP^{5LO}**, and **ba**CD. In (a), vials 1 and 2 contain solutions of **AgNP^{6LA}**, vials 5 and 6 solutions of **AuNP^{5LO}**, and vials 3 and 4 mixtures of these nanoparticles in water. The aqueous **ba**CD solution was added to vials 2, 4, and 6, while an equivalent amount of water was added to vials 1, 3, and 5. The TEM images in (c) illustrate the aggregation state after bis(cyclodextrin) addition (part of these images and graphs are also shown in Fig. 2 of the main article).

(a) Start



1000 μM
+1 h



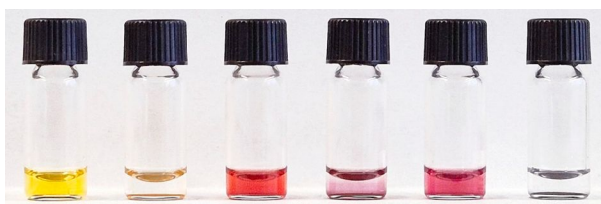
1000 μM
+3 d



1500 μM
+15 min

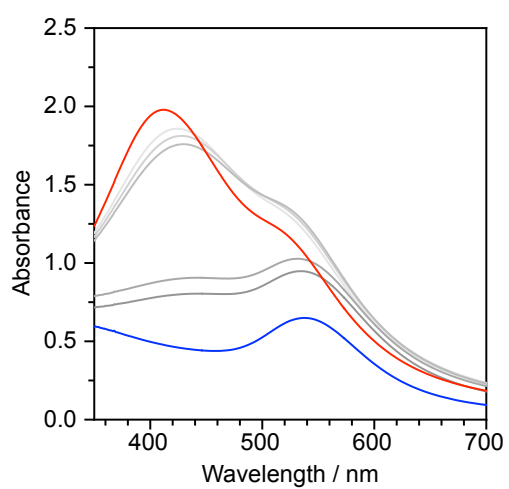


1500 μM
+24 h

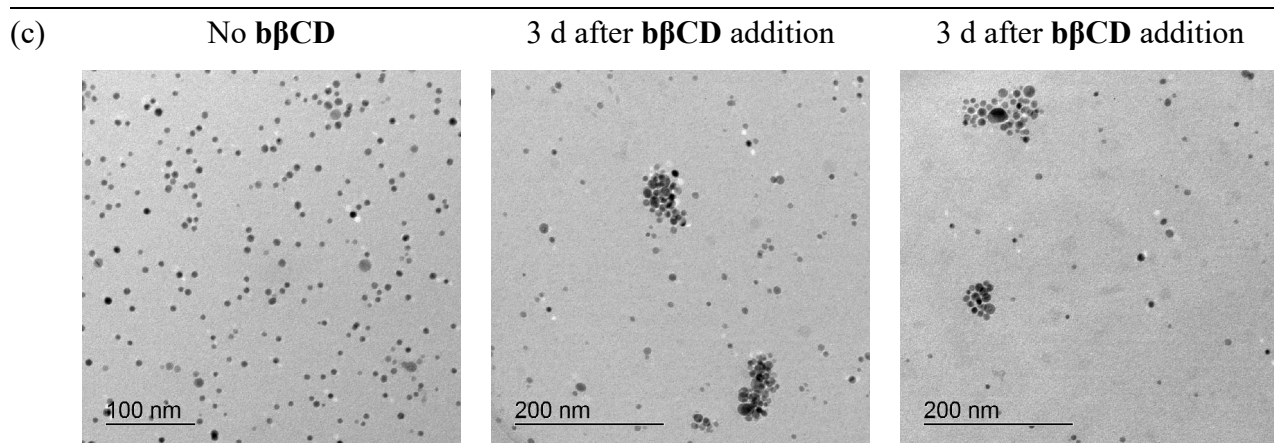


1 2 3 4 5 6

(b)



— 1500 μM , +24 h
— 1000 μM , +15 min
— 1000 μM , +2 h
— 1000 μM , +4 h
— 1000 μM , +3 d
— 1500 μM , +15 min
— 0 μM



Average diameter of the non-aggregated nanoparticles: 8.0 ± 1.5 nm

The solution containing **AgNP^{6LA}** gradually became colourless in the presence of **bβCD** while the colour of the **AuNP^{5LO}** solution remained unchanged. Precipitation of the latter nanoparticles only occurred at a higher concentration of the bis(cyclodextrin). In the UV-vis spectroscopic binding study, the SPR band of **AgNP^{6LA}** decreased in intensity until no clear band was visible anymore. The SPR band of **AuNP^{5LO}** persisted longer. The TEM images in (c) illustrate that only part of the nanoparticles initially aggregated in the presence of the bis(cyclodextrin).

Figure S29: Visual (a) and UV-vis spectroscopic binding study (b) for the combination **AgNP^{6LA}**, **AuNP^{5LO}**, and **bβCD**. In (a), vials 1 and 2 contain solutions of **AgNP^{6LA}**, vials 5 and 6 solutions of **AuNP^{5LO}**, and vials 3 and 4 mixtures of these nanoparticles in water. The aqueous **bβCD** solution was added to vials 2, 4, and 6, while an equivalent amount of water was added to vials 1, 3, and 5. The TEM images in (c) illustrate the aggregation state after bis(cyclodextrin) addition.

(a) Start



500 μM
+24 h



1000 μM
+12 h



1500 μM
+2 h

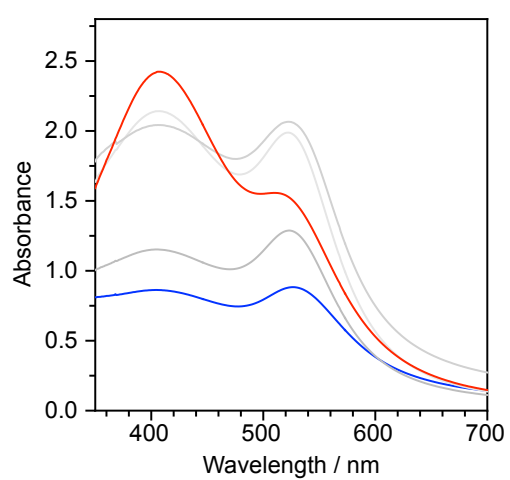


1500 μM
+24 h

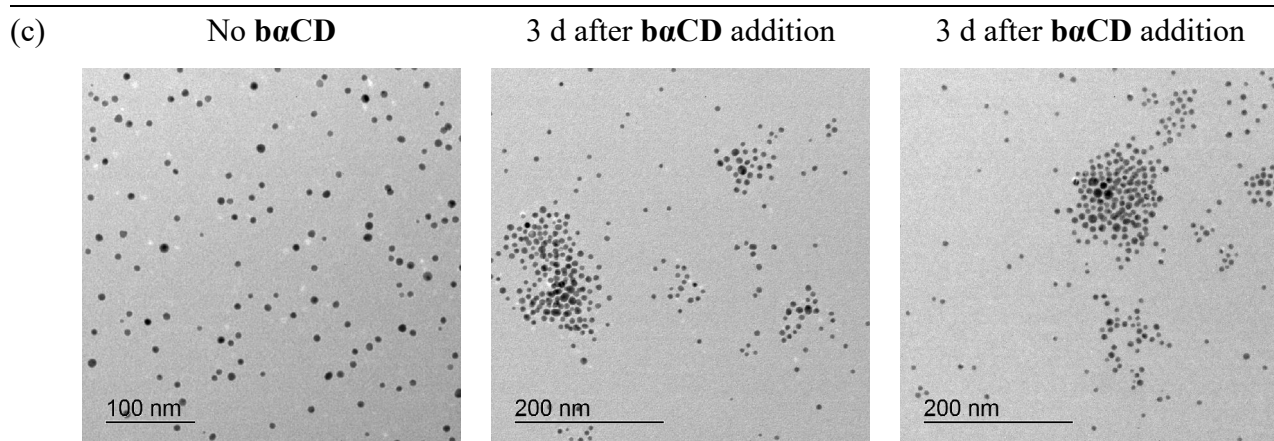


1 2 3 4 5 6

(b)



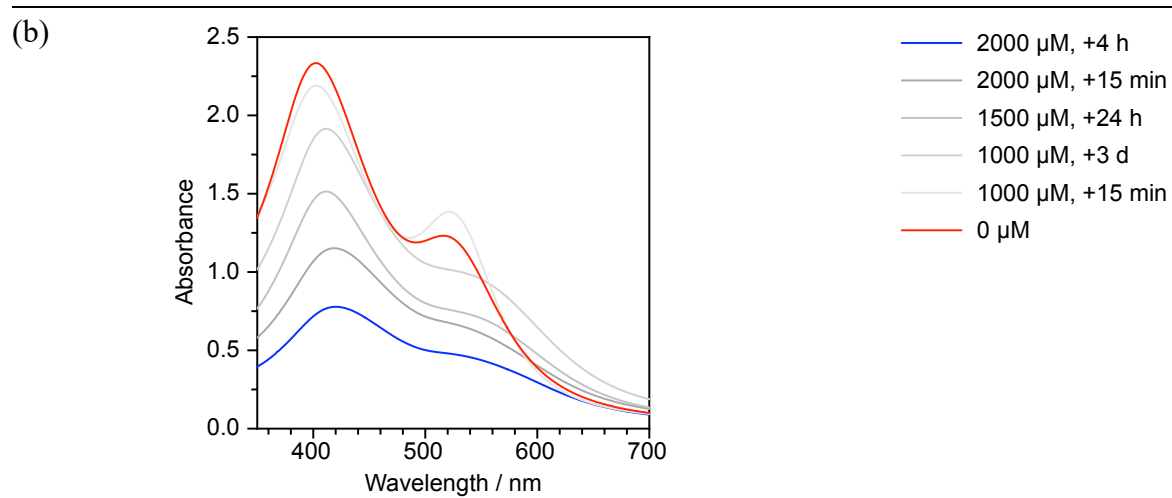
— 1500 μM , +24 h
— 500 μM , +3 d
— 750 μM , +24 h
— 750 μM , +3 d
— 0 μM

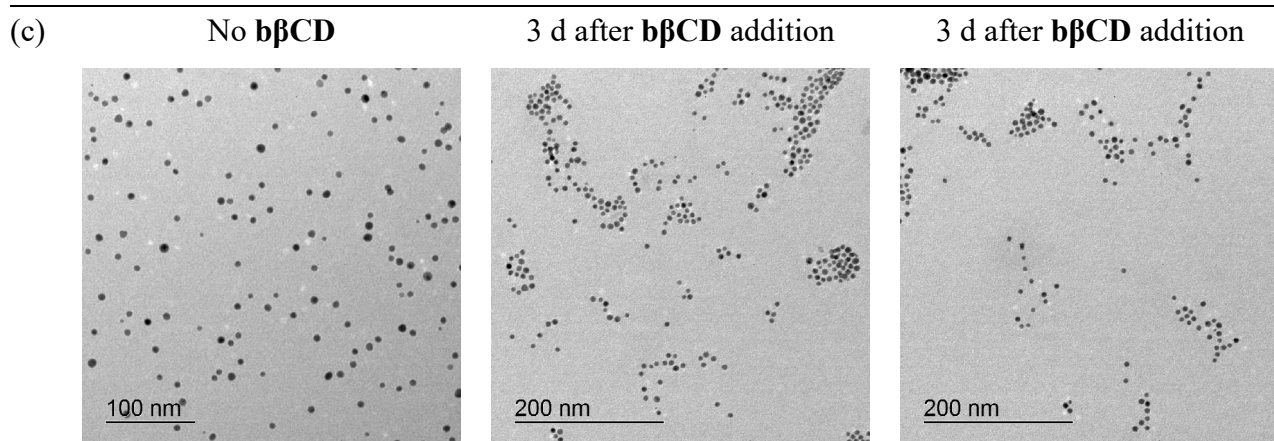


Average diameter of the non-aggregated nanoparticles: 6.7 ± 1.5 nm

The solution containing **AgNP**^{6LO} gradually became colourless in the presence of **ba**CD while the colour of the **AuNP**^{6LA} solution remained unchanged. Precipitation of the latter nanoparticles only occurred at a higher concentration of the bis(cyclodextrin). In the UV-vis spectroscopic binding study, the SPR band of **AgNP**^{6LO} decreased in intensity preferentially until no clear band was visible anymore (at the moment, we have no explanation for the increase of the gold SPR band after the first two additions). The SPR band of **AuNP**^{6LA} persisted longer. The TEM images in (c) illustrate that only part of the nanoparticles initially aggregated in the presence of the bis(cyclodextrin).

Figure S30: Visual (a) and UV-vis spectroscopic binding study (b) for the combination **AgNP**^{6LO}, **AuNP**^{6LA}, and **ba**CD. In (a), vials 1 and 2 contain solutions of **AgNP**^{6LO}, vials 5 and 6 solutions of **AuNP**^{6LA}, and vials 3 and 4 mixtures of these nanoparticles in water. The aqueous **ba**CD solution was added to vials 2, 4, and 6, while an equivalent amount of water was added to vials 1, 3, and 5. The TEM images in (c) illustrate the aggregation state after bis(cyclodextrin) addition.





Average diameter of the non-aggregated nanoparticles: 7.8 ± 2.4 nm

The solution containing **AuNP^{6LA}** turned blue and then became colourless in the presence of **bβCD** while the colour of the **AgNP^{6LO}** solution remained unchanged. Precipitation of the latter nanoparticles only occurred at a higher concentration of the bis(cyclodextrin). In the UV-vis spectroscopic binding study, the SPR band of **AuNP^{6LA}** shifted to longer wavelengths and decreased in intensity until no clear band was visible anymore. The SPR band of **AgNP^{6LO}** persisted longer. The TEM images in (c) illustrate that only part of the nanoparticles initially aggregated in the presence of the bis(cyclodextrin).

Figure S31: Visual (a) and UV-vis spectroscopic binding study (b) for the combination **AgNP^{6LO}**, **AuNP^{6LA}**, and **bβCD**. In (a), vials 1 and 2 contain solutions of **AgNP^{6LO}**, vials 5 and 6 solutions of **AuNP^{6LA}**, and vials 3 and 4 mixtures of these nanoparticles in water. The aqueous **bβCD** solution was added to vials 2, 4, and 6, while an equivalent amount of water was added to vials 1, 3, and 5. The TEM images in (c) illustrate the aggregation state after bis(cyclodextrin) addition.

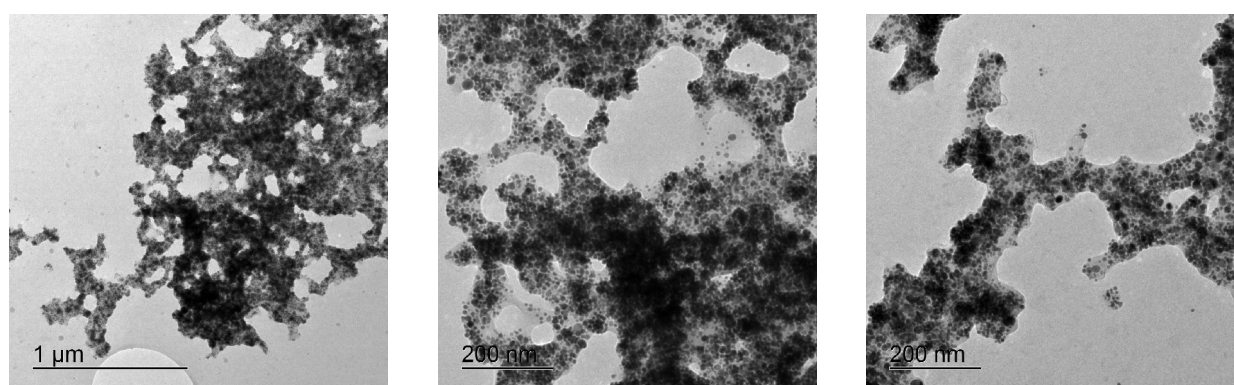


Figure S32: TEM images of a mixture of **AuNP^{6LA}** and **AgNP^{6LO}** after the simultaneous addition of **βαCD** and **bβCD**.



Start				
total bis(cyclodextrin) concentration 1500 μ M +3 d				
Vial #	1	2	3	4

Figure S33: Effects of the addition of **α CD** (vial 2), **β CD** (vial 4), and a mixture of **α CD** and **β CD** (vial 3) on an aqueous solution of **AgNP^{6LA}** and **AuNP^{5LO}** under the conditions specified. In vial 1, an equivalent amount of water was added to the same nanoparticle mixture.



Start				
total bis(cyclodextrin) concentration 1500 μ M +3 d				
Vial #	1	2	3	4

Figure S34: Effects of the addition of **α CD** (vial 2), **β CD** (vial 4), and a mixture of **α CD** and **β CD** (vial 3) on an aqueous solution of **AgNP^{6LO}** and **AuNP^{6LA}** under the conditions specified. In vial 1, an equivalent amount of water was added to the same nanoparticle mixture.

References

1. K. Kai, H. Fujii, R. Ikenaka, M. Akagawa and H. Hayashi, *Chem. Commun.*, 2014, **50**, 8586–8589.
2. J. Hu, F. Yang and M. Huang, *Adv. Mat. Res.*, 2011, **391-392**, 1159–1163.
3. J. Bartl, L. Reinke, M. Koch and S. Kubik, *Chem. Commun.*, 2020, **56**, 10457–10460.
4. S. Marchesan and D. Macmillan, *Chem. Commun.*, 2008, 4321–4323.
5. H. Zinner, G. Sych and W. Ludwig, *J. Prakt. Chem.*, 1962, **17**, 147–153.
6. K. Hamasaki, H. Ikeda, A. Nakamura, A. Ueno, F. Toda, I. Suzuki and T. Osa, *J. Am. Chem. Soc.*, 1993, **115**, 5035–5040.
7. C. Hübler, *Chem. Methods* 2022, **2**, e202200006.
8. N. R. Jana, L. Gearheart and C. J. Murphy, *Langmuir*, 2001, **17**, 6782–6786.
9. J. A. Creighton, C. G. Blatchford and M. G. Albrecht, *J. Chem. Soc., Faraday Trans. 2*, 1979, **75**, 790–798.